DOI: 10.1002/asia.200600355

Toward Electrochemically Controllable Tristable Three-Station [2]Catenanes

Taichi Ikeda,[a] Sourav Saha,[a] Ivan Aprahamian,[a] Ken C.-F. Leung,[a] Adides Williams,[a] Wei-Qiao Deng,[b] Amar H. Flood,[a, c] William A. Goddard III,[b] and J. Fraser Stoddart*[a]

Abstract: Encouraged by the prospect of producing an electrochemical, color-switchable red–green–blue (RGB) dye compound, we have designed, synthesized, and characterized two three-station [2]catenanes. Both are composed of macrocyclic polyethers containing three π-electron-rich stations, which act as recognition sites for a π-electron-deficient tetracationic cyclophane. The molecular structures of the two three-station [2]catenanes were characterized fully by mass spectrometry and ^{1}H NMR spectroscopy. To anticipate the relative occupancies of the three stations in each [2]catenane by the cyclophane, model compounds with the same constitutions in the vicinity of the stations were synthesized. The relative ground-state populations of the three stations occupied in both [2]catenanes were estimated from the thermodynamic parameters for 1:1 complexes between all these model compounds and the cyclophane, obtained from isothermal titration calorimetry (ITC). The electrochemical and electromechanical properties of the three-station [2]catenanes were analyzed by cyclic voltammetry (CV), differential pulse voltammetry (DPV), and spectroelectrochemistry (SEC). The first three-station [2]catenane was found to behave like a bistable system, whereas the second can be described as a quasi-tristable system.

Keywords: catenanes · crown ethers · electrochemistry · molecular devices · thermodynamics

Introduction

Supramolecular chemistry has alerted many chemists to the importance of weak noncovalent interactions[1] and has led to the design and synthesis of mechanically interlocked compounds, such as rotaxanes and catenanes, using a template-directed protocol.[2] Mechanically interlocked compounds[3] that consist of a dumbbell-shaped component and a ring component are known as [2]rotaxanes, whereas those composed of a pair of mutually interlocked ring components are called [2]catenanes. Although the first generation[4] of [2]rotaxanes and [2]catenanes with multiple recognition sites were nondegenerate with respect to the relative positioning of their components, subsequent designs[5] incorporated bistability, which was eventually expressed synthetically as two equilibrating states with very different free energies, that is, one state of the molecule is populated to a much greater extent than the other one. The next step in the conceptual development of the field was the realization of switchable, bistable [2]rotaxanes and [2]catenanes, in which the relative positioning of the components can be elevated from the ground state to a metastable one as a result of chemical,[6] electrochemical,[7] optical,[8] or a collection of some of these stimuli,[9] thus creating the fundamental basis for the construction of simple two-state switches. This realization and subsequent research activity—focused on bistable rotaxanes and catenanes—has moved the challenge, at least temporarily, away from synthesis to the creation of molecular devices.[10]

[a] Dr. T. Ikeda, Dr. S. Saha, Dr. I. Aprahamian, Dr. K. C.-F. Leung, A. Williams, Dr. A. H. Flood, Prof. J. F. Stoddart
The California NanoSystems Institute
and
Department of Chemistry and Biochemistry
University of California, Los Angeles
405 Hilgard Avenue, Los Angeles, CA 90095-1569 (USA)
Fax: (+1) 310-206-5621
E-mail: stoddart@chem.ucla.edu

[b] Dr. W.-Q. Deng, Prof. W. A. Goddard III
Materials and Process Simulation Center
Division of Chemistry and Chemical Engineering
California Institute of Technology
Pasadena, CA 91125 (USA)

[c] Dr. A. H. Flood
Current Address:
Department of Chemistry, Indiana University
800 East Kirkwood Avenue, Bloomington, IN 47405 (USA)

The mechanically interlocked donor–acceptor compounds we have been developing in recent years[11] in the shape of two-station [2]rotaxanes[12] and [2]catenanes[13] are usually composed of a tetracationic cyclophane, cyclobis(paraquat-*p*-phenylene)[14] ($CBPQT^{4+}$), and a dumbbell or another ring component, respectively, encompassing two stations or recognition sites for $CBPQT^{4+}$, principally tetrathiafulvalene[15] (TTF) and 1,5-dioxynaphthalene[16] (DNP) units. In this donor–acceptor system, the π-electron-poor $CBPQT^{4+}$ ring interacts with the π-electron-rich recognition sites TTF (more so) and DNP (less so) by means of charge-transfer (CT) interactions in part.[11–17] Although other weak interactions, such as π····π stacking and C–H····π, C–H····O, and van der Waals interactions play a crucial role in stabilizing the $CBPQT^{4+}$ ring around the recognition sites,[13,16,17] the CT interactions confer useful electrochemical and electrooptical properties on these systems.[12,13,18] A series of incremental advances, made over almost two decades now to unleash the potential of these bistable [2]rotaxanes and [2]catenanes, has positioned these compounds as leading candidates[18] for the fabrication of molecular electronic devices and nanoelectromechanical systems (NEMS).

So far, our extensive research and development work[15] has been limited to bistable, two-station [2]rotaxanes[12] and [2]catenanes.[13] The time is now ripe, however, to extend our research effort to encompass tristable, three-station [2]catenanes. Employing a different recognition motif, Leigh et al.[19] reported examples of tristable, three-station [2]- and [3]catenanes in which one of the rings can be made to undergo unidirectional circumrotation in a stepwise manner. If we can realize tristable, donor–acceptor, three-station [2]catenanes using the π-electron-accepting $CBPQT^{4+}$ rings with π-electron-donating recognition sites (stations) in the other ring, we stand a good chance of uncovering electrochemical, electrooptical, and electromechanical properties that are not attainable in bistable two-station [2]rotaxanes and [2]catenanes.

Recently, we suggested[20] that an electrochemically controllable red–green–blue (RGB) [2]catenane could be the basis for constructing a different kind of electrochromic device (Figure 1).[21] In such a system, we might expect that a change in location of the $CBPQT^{4+}$ ring between three π-electron-donating stations might generate three different colors (RGB) based on the different CT interactions between the $CBPQT^{4+}$ ring and these three distinct, carefully chosen stations. To achieve tristability, a three-station [2]catenane must satisfy the following two requirements. 1) As the partitioning of the occupation on three different stations by the $CBPQT^{4+}$ ring reflects the relative free energies of the three states, the association constants (K_a) for the $CBPQT^{4+}$ ring and the three stations must differ by at least one order of magnitude.[22] 2) The order of magnitude of these K_a values must be coupled judiciously to the oxidation potentials of the three different stations, that is, the station with the largest K_a value must have the smallest oxidation potential for it to address the tristable [2]catenane electrochemically. In an attempt to satisfy these two requirements

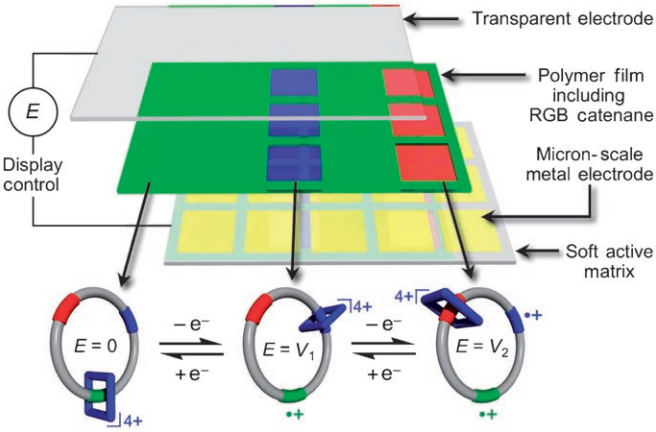

Figure 1. The proposed design for electronic paper displays based on the electrochromism of electrochemically controllable three-station [2]catenanes. The control voltage is applied between the transparent electrode and the soft active matrix to manipulate the color switch in the pixel layer, which is impregnated with three-station [2]catenanes capable of exhibiting RGB colors in response to the applied voltage. The RGB colors originate from the CT absorption bands between the tetracationic cyclophane and the three stations on the macrocyclic polyethers.

and develop the concept of an RGB [2]catenane, we employed DFT calculations at the outset.[20]

In the proposed design (Figure 2a), TTF, DNP, and difluorinated benzidine (DFBZ) units were identified as the

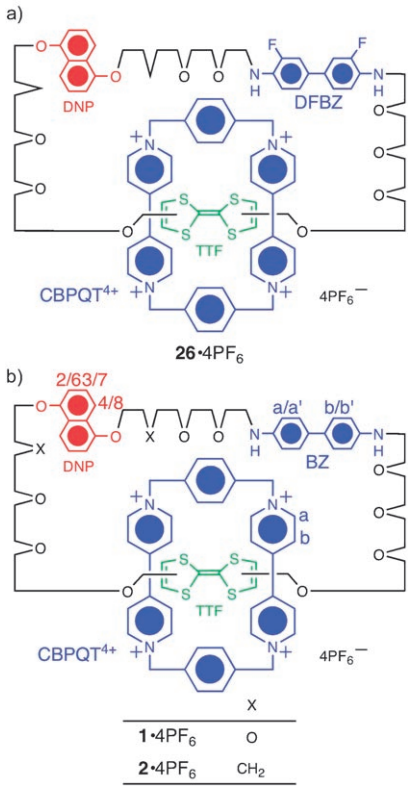

Figure 2. Structural formulae of a) the RGB [2]catenane **26**·4 PF_6 and b) the three-station [2]catenanes **1**·4 PF_6 and **2**·4 PF_6. The abbreviation for each station and the labeling scheme for the NMR spectral assignments are also depicted.

different stations to be incorporated into the π-electron-rich macrocyclic polyether. Furthermore, we gave ourselves the liberty to replace the two closest ether oxygen atoms around the DNP unit to exchange the relative magnitudes of the K_a values.[23] Towards this theoretically optimized design, we identified two three-station [2]catenanes **1**·4PF$_6$ and **2**·4PF$_6$ as prototypes in which the benzidine (BZ) unit is employed as a station instead of the DFBZ unit. In the [2]catenane **1**·4PF$_6$, the three stations are linked by tetraethyleneglycol chains. The binding constants of the CBPQT^{4+} ring with oligoethyleneglycol-tethered TTF, DNP, and BZ units were already reported as 380000, 36400, and 1100 M^{-1} (MeCN, 298 K), respectively.[24,25] Although the relative binding affinities satisfy the first requirement mentioned above, the oxidation potential of the BZ unit is substantially smaller than that of DNP. Thus, we did not expect **1**·4PF$_6$ to exhibit tristability. The synthesis of **1**·4PF$_6$, however, was viewed as a practice run for the synthesis of **2**·4PF$_6$. Furthermore, it was anticipated that **1**·4PF$_6$ would provided a reference point from which to assess **2**·4PF$_6$. In **2**·4PF$_6$, the two oxygen atoms closest to the DNP unit were exchanged for methylene groups to adjust the K_a values of the DNP unit.[23] As this structural modification should lead to the desired consistency between ordering of the K_a values and ordering of the oxidation potentials, **2**·4PF$_6$ was considered to be a promising candidate to exhibit tristability. Herein, we report some thermodynamic data for 1:1 complexes formed between CBPQT^{4+} and model compounds for the recognition units in **1**·4PF$_6$ and **2**·4PF$_6$. Armed with background information, we describe the synthesis and characterization by UV/Vis and ^{1}H NMR spectroscopy. The electrochemical and electromechanical behavior of **1**·4PF$_6$ and **2**·PF$_6$ are compared and contrasted based on the results obtained from cyclic voltammetry, differential pulse voltammetry, and spectroelectrochemistry.

Results and Discussion

Thermodynamic Binding Data for Model Compounds

In this investigation, we employed TTF,[15] BZ,[25] and DNP[16] units as binding sites for the CBPQT^{4+} ring.[14] We identified two three-station [2]catenanes in which a crown ether incorporating TTF, BZ, and DNP stations is interlocked with a CBPQT^{4+} ring (Figure 2b). To determine the relative preferences for encirclement of these three stations by the ring in **1**·4PF$_6$ and **2**·4PF$_6$, the binding strengths of some model guests with CBPQT·4PF$_6$ as the host were obtained from measurements carried out in MeCN with isothermal titration calorimetry (ITC). This method is convenient for obtaining the thermodynamic parameters (ΔH, ΔS, and ΔG) associated with complex formation at a given temperature.[1c,26] The structural formulae of the model guests and CBPQT^{4+} are illustrated in Figure 3. The thermodynamic binding data for the tetraethyleneglycol-disubstituted TTF and DNP fragments in MeCN (TTF-TEG: K_a = 416000 M^{-1}; DNP-TEG: K_a = 43900 M^{-1}) are comparable

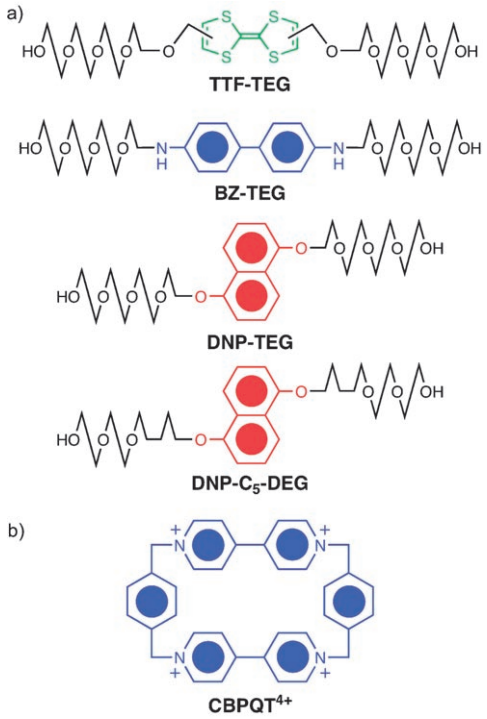

Figure 3. a) Structural formulae of the series of model guests TTF-TEG, BZ-TEG, DNP-TEG, and DNP-C$_5$-DEG. b) Structural formula of the host, cyclobis(paraquat-*p*-phenylene) (CBPQT^{4+}).

with those obtained for the diethyleneglycol-disubstituted TTF and DNP fragments (TTF-DEG: K_a = 380000 M^{-1}; DNP-DEG: K_a = 36400 M^{-1}) in a previous investigation.[24] The binding constant for tetraethyleneglycol-disubstituted BZ (BZ-TEG) with CBPQT·4PF$_6$ is 1910 M^{-1}. This K_a value is comparable with that obtained previously with a UV/Vis titration method and a closely related model guest, namely, triethyleneglycol-disubstituted BZ (K_a = 1100 M^{-1}).[25] These ITC results indicate that the smaller enthalpy gain when CBPQT^{4+} binds BZ-TEG (−42.3 kJ mol^{-1}) compared to when it binds either TTF-TEG (−60.9 kJ mol^{-1}) or DNP-TEG (−65.4 kJ mol^{-1}) means that the CBPQT^{4+} ring in both [2]catenanes will encircle preferentially the TTF and DNP units rather than BZ. It was reported that the introduction of ethyleneglycol chains improves the binding ability of TTF and DNP derivatives[23,24] on account of stabilizing C−H···O interactions[17] present in their 1:1 complexes with CBPQT^{4+}. In the case of BZ, the binding constant for unsubstituted BZ (K_a = 1044 M^{-1}) and triethyleneglycol-disubstituted BZ (K_a = 1100 M^{-1}) are the same[25] within experimental error, suggesting that the ethyleneglycol chains do not lead to an increase in binding energy in the case of BZ derivatives.[23] Thus, the smaller enthalpy gain of BZ-TEG relative to TTF-TEG and DNP-TEG during 1:1 complexation with CBPQT·4PF$_6$ arises from much weaker interactions between the BZ-TEG ethyleneglycol chains and the CBPQT^{4+} ring.

The disubstituted DNP-C$_5$-DEG (K_a = 122 M^{-1}) (Figure 3) has a much smaller binding constant with CBPQT·4PF$_6$

than does DNP-TEG ($K_a = 43\,900\ M^{-1}$). The K_a value for DNP-C_5-DEG is comparable with that[24] for unsubstituted DNP ($K_a = 440\ M^{-1}$). The ether oxygen atoms of DNP-TEG contribute to the stabilization of the 1:1 complex with $CBPQT^{4+}$ by means of C–H···O interactions.[17] X-ray crystallographic data for the 1:1 complex formed between DNP-TEG and CBPQT·4PF_6 indicate that the second and third oxygen atoms distant from the 1,5-dioxynaphthalene ring system are involved in C–H···O interactions with the $CBPQT^{4+}$ ring.[16] The small K_a value for DNP-C_5-DEG and CBPQT·4PF_6 reveals that exchanging the second-closest oxygen atom for a methylene group is highly effective in reducing the binding to the $CBPQT^{4+}$ ring. Although both three-station [2]catenanes contain the same three stations—namely, TTF, BZ, and DNP—the attraction of the $CBPQT^{4+}$ ring for the DNP stations in **1**·4PF_6 and **2**·4PF_6 is different as a result of the different constitutions in the immediate vicinities of the DNP stations.

The UV/Vis spectra of the 1:1 complexes (Figure 4a) formed between CBPQT·4PF_6 and DNP-TEG, BZ-TEG, and TTF-TEG in MeCN (concentrations of complexes = 1, 1, and 0.1 mM, respectively) are shown in Figure 4b. The absorption maxima are at about 540, 620, and 820 nm, respectively. The colors of the three different stations are shown in Figure 4c. The results augur well for the design of a three-station [2]catenane that is tristable and electrochemically controllable.

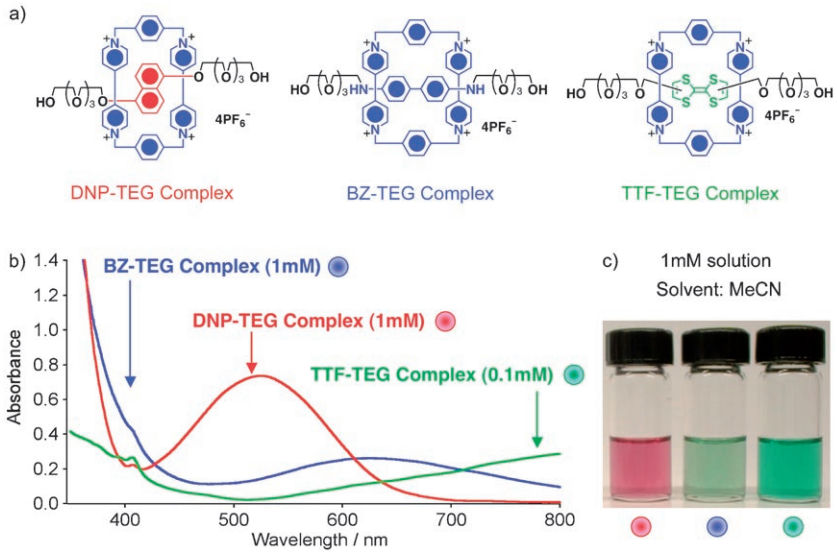

Figure 4. a) Structural formulae, b) UV/Vis spectra, and c) colors of solutions in MeCN of the complexes formed between π-electron-rich DNP-TEG (red), BZ-TEG (blue), and TTF-TEG (green) polyether chains and the π-electron-deficient CBPQT·4PF_6.

Synthesis of the First Three-Station [2]Catenane

The [2]catenane **1**·4PF_6 was prepared according to the routes outlined in Schemes 1 and 2. The synthesis of the crown ethers **5** and **16** are described in Scheme 1. The secondary amine groups of tetraethyleneglycol-disubstituted benzidine **10**[25a] were Boc-protected. Di-*tert*-butyl dicarbonate reacted selectively with the secondary amine groups and not at all with the terminal hydroxy groups of **10**, which were subsequently tosylated to afford the monotosylate **12**. Alkylation of the tetraethyleneglycol-monosubstituted 1,5-dioxynaphthalene **13**[27] with **12** gave the diol **14**, which was converted into ditosylate **15**. The Boc-protected macrocycle **5** was obtained by reaction of the **15** with TTF diol (TTF-OH)[28] in the presence of Cs_2CO_3 and NaH and heating under reflux in THF for two days.[13,29] The Boc-protected [2]catenane **3**·4PF_6 was self-assembled (Scheme 2) under high-pressure conditions (12 kbar) in DMF at room temperature by using **5** as the template for the formation of the $CBPQT^{4+}$ ring from **7**·2PF_6 and 1,4-bis(bromomethyl)benzene (**8**), followed by counterion exchange (NH_4PF_6). Finally, the three-station [2]catenane **1**·4PF_6 was obtained by Boc-deprotection of **3**·4PF_6 with TsOH under reflux in Me_2CO, followed by counterion exchange (NH_4PF_6). The overall yield of **1**·4PF_6 following these two steps amounts to only 46% because of the decomposition of TTF and BZ under the acidic conditions of the deprotection step.

Synthesis of the Second Three-Station [2]Catenane

The [2]catenane **2**·4PF_6 was synthesized according to the routes outlined in Schemes 3 and 2. DNP was alkylated with 5-bromopentanol in MeCN in the presence of K_2CO_3 to afford the diol **17**. Further alkylation of **17** with 2-[2-(2-chloroethoxy)ethoxy]-tetrahydropyran[13a] (**18**) in THF in the presence of NaH and NaI and subsequent deprotection of the THP group with PPTS gave the diol **20**.[30] The monotosylated **21**, prepared from **20**, was coupled with the tetraethyleneglycol-monosubstituted derivative **22** in PhMe to afford the diol **23**. Following Boc-protection of the secondary amine groups in **23**, the terminal hydroxy groups of **24** were tosylated. The Boc-protected macrocycle **6** was prepared from the ditosylate **25** and TTF-OH[28] in the presence of Cs_2CO_3 and NaH by heating under reflux in THF for two days.[13,29] The Boc-protected [2]catenane **4**·4PF_6 was self-assembled (Scheme 2) under high-pressure conditions (12 kbar) in DMF at room temperature by using **6** as the template for the formation of the $CBPQT^{4+}$ ring from **7**·2PF_6 and **8**, followed by counterion exchange (NH_4PF_6). Finally, the three-station [2]catenane **2**·4PF_6 was obtained in 50% yield after Boc-deprotection of **4**·4PF_6 with TsOH

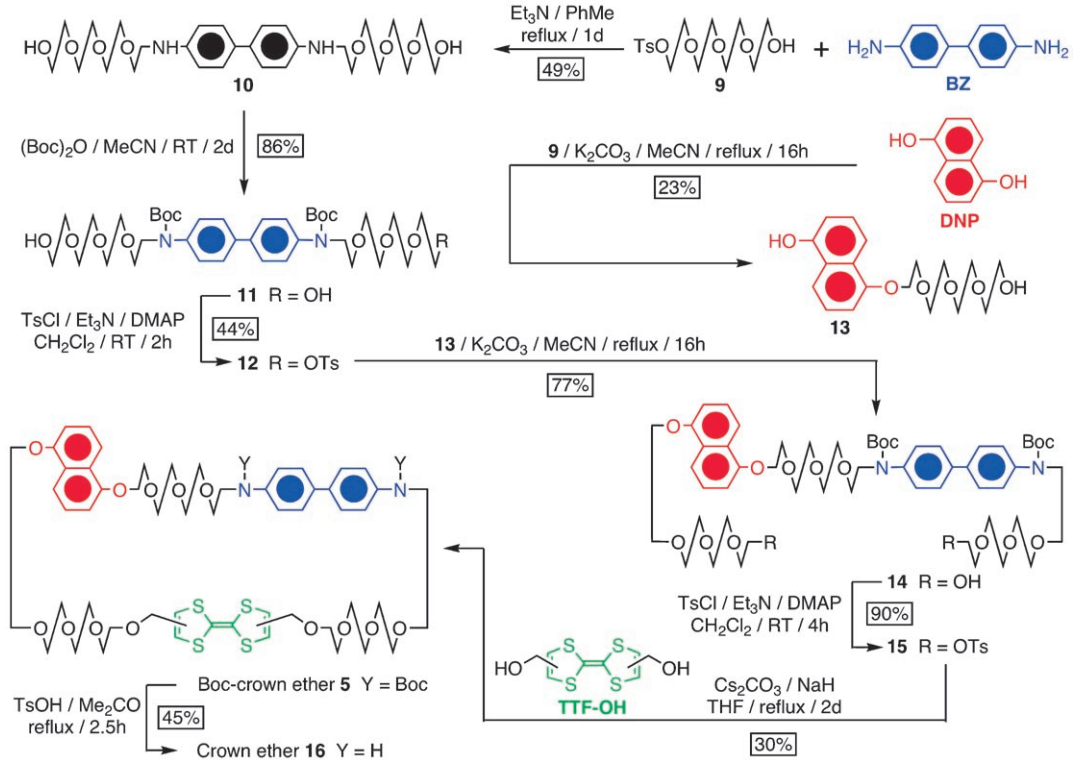

Scheme 1. Synthetic route to the Boc-crown ether **5** employed in the template-directed synthesis of the three-station [2]catenane **1**·4PF$_6$. Boc = *tert*-butoxycarbonyl, DMAP = 4-dimethylaminopyridine, Ts = *p*-toluenesulfonyl; d = days.

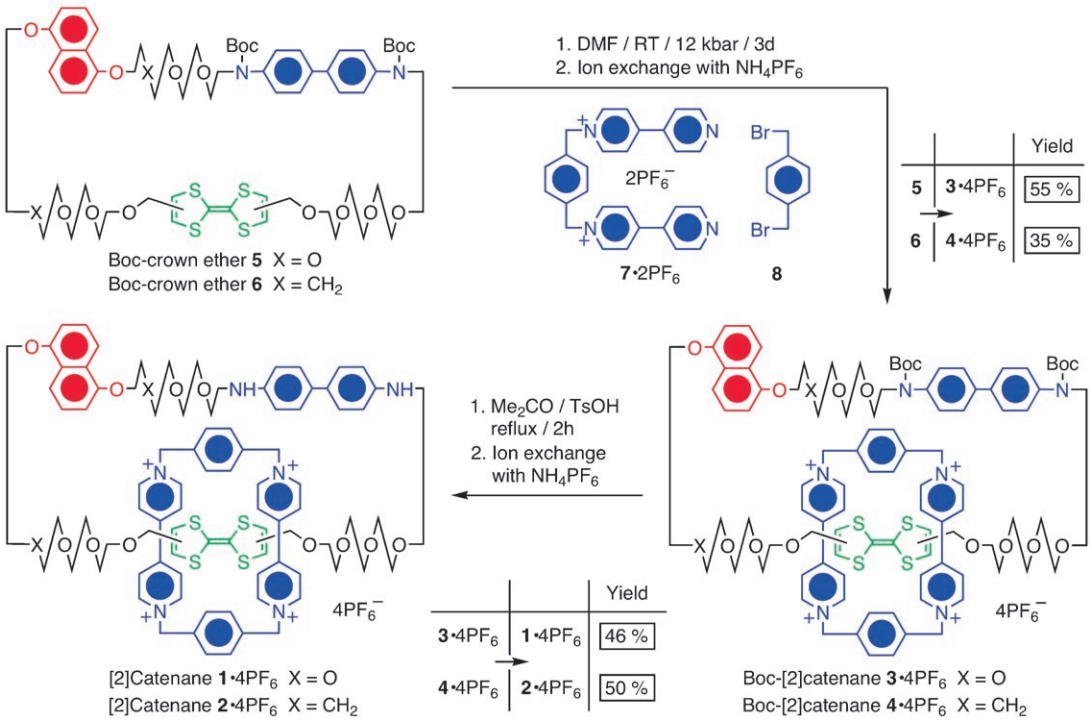

Scheme 2. The template-directed syntheses of the three-station [2]catenanes **1**·4PF$_6$ and **2**·4PF$_6$. DMF = *N*,*N*-dimethylformamide, THP = 2-tetrahydropyranyl.

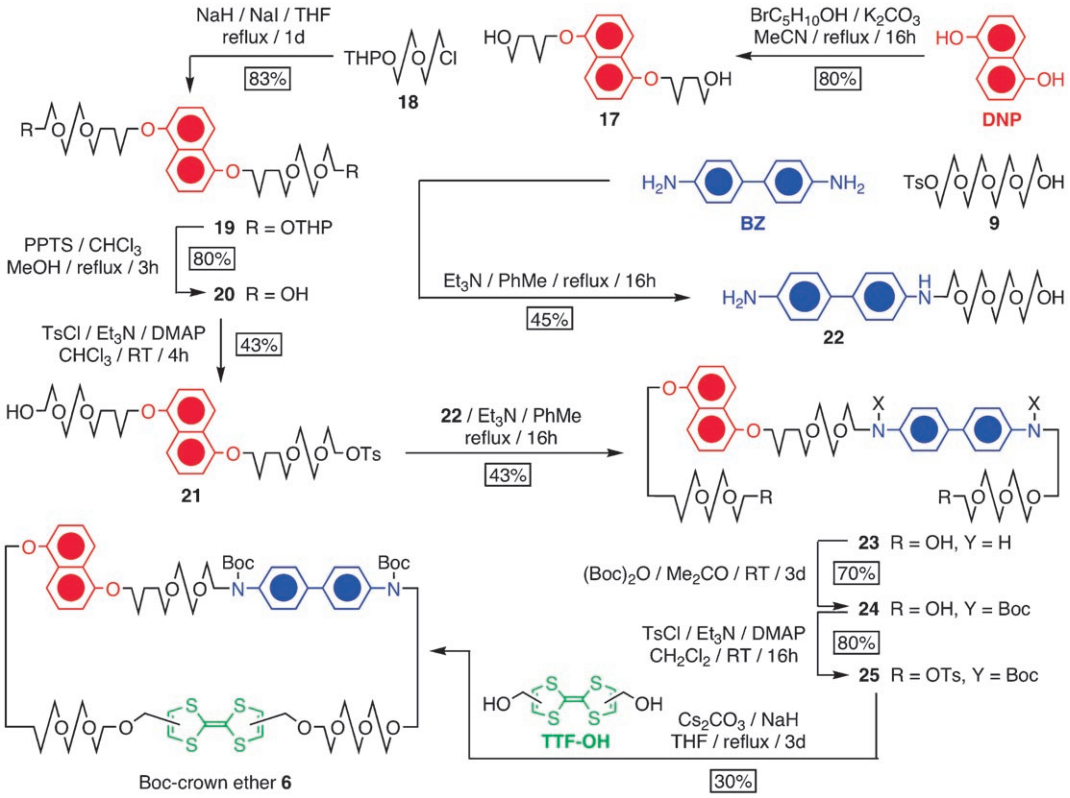

Scheme 3. Synthetic route to the Boc-crown ether **6** employed in the template-directed synthesis of the three-station [2]catenane **2**·4PF_6. PPTS = pyridinium *p*-toluenesulfonate.

under reflux in Me_2CO, followed by counterion exchange (NH_4PF_6).

UV/Vis Absorption Spectra of the Three-Station [2]Catenanes

The absorption spectra recorded for **1**·4PF_6 and **2**·4PF_6 are superimposed in Figure 5. Although these three-station [2]catenanes have the same chromophores (TTF, BZ, DNP, and $CBPQT^{4+}$), the absorption spectra are not identical. The color difference is significant enough to be recognized by the eye (Figure 5, inset). The [2]catenane **1**·4PF_6 is a darker green than its analogue **2**·4PF_6. The absorption bands in the visible region arise from the CT bands between the π-electron-donor stations and the π-electron-accepting $CBPQT^{4+}$ ring.[12,17,21,25] It was reported that the CT bands for DNP→$CBPQT^{4+}$ and TTF→$CBPQT^{4+}$ appear as broad absorptions centered at 530 and 840 nm, respectively.[21] The differences in the absorption of the CT bands in **1**·4PF_6 and **2**·4PF_6 are significant in the region of these two well-separated bands (Figure 5). The absorption intensities of the DNP→$CBPQT^{4+}$ and TTF→$CBPQT^{4+}$ CT bands for **1**·4PF_6 are more and less, respectively, than those for **2**·4PF_6. These differences indicate that the proportion of the $CBPQT^{4+}$ ring residing on the DNP unit in **1**·4PF_6 is more than that in **2**·4PF_6. When the binding affinities of all three stations towards the $CBPQT^{4+}$ ring are taken into account, this behavior is entirely reasonable. Assuming that the partitioning of the $CBPQT^{4+}$ ring between the three stations reflects the thermodynamic properties of the guest compounds listed in Table 1, we can estimate the population of the $CBPQT^{4+}$ ring on each station in the two [2]catenanes. In the case of **1**·4PF_6, the populations of the $CBPQT^{4+}$ ring on the TTF, BZ, and DNP stations are 90.1, 0.4, and 9.5%, respectively. In the case of **2**·4PF_6, the populations are 99.5, 0.5, and 0.0%, respectively. Hence, a significant amount of the $CBPQT^{4+}$ ring is present on the DNP station in **1**·4PF_6, but absent, to all intents and purposes, in **2**·4PF_6, in which

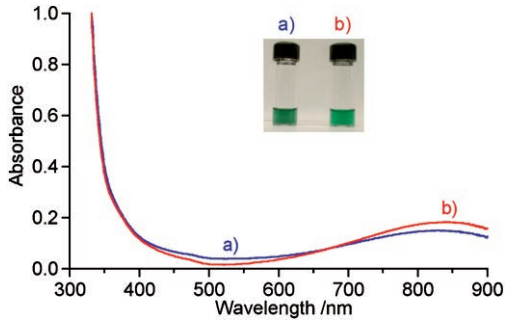

Figure 5. UV/Vis spectra of a) **1**·4PF_6 and b) **2**·4PF_6 in MeCN. Inset: A photograph of these solutions. The concentrations of the solutions for the absorption measurement and the photograph were 4.0×10^{-5} and 1.0×10^{-3} M, respectively.

Table 1. Thermodynamic binding data corresponding to the complexation between $CBPQT^{4+}$ and the individual components of the three-station catenanes in MeCN determined by ITC at 298 K.

Guest	ΔH[a] [kJ mol^{-1}]	$T\Delta S$[b] [kJ mol^{-1}]	ΔG[c] [kJ mol^{-1}]	K_a[d] [$\times 10^3$ M^{-1}]
TTF-TEG[e]	-60.9 ± 0.2	-28.7	-32.1	416.0 ± 23.0[i]
BZ-TEG[f]	-42.3 ± 1.0	-23.6	-18.7	1.91 ± 0.09[j]
DNP-TEG[g]	-65.4 ± 0.2	-38.8	-26.5	43.9 ± 0.76[k]
DNP-C_5-DEG[h]	-57.3 ± 0.3	-45.3	-11.9	0.122 ± 0.001

[a] Enthalpy change of the reaction. [b] Calculated from the ΔH and ΔG values by using the equation $\Delta G = \Delta H - T\Delta S$. [c] Calculated from the fitted value of K_a by using the equation $\Delta G = -RT\ln K_a$. [d] Obtained from curve-fitting to the binding isotherm. Fits were performed with the software provided by Microcal LLC, and the stoichiometry of all complexes was between 0.97 and 1.03, indicating that a 1:1 complex was formed. [e] Concentrations: TTF-TEG 3.2 mM, $CBPQT^{4+}$ 0.4 mM. [f] Concentrations: BZ-TEG 9.0 mM, $CBPQT^{4+}$ 1.0 mM. [g] Concentrations: DNP-TEG 4.0 mM, $CBPQT^{4+}$ 0.40 mM. [h] Concentrations: DNP-C_5-DEG 18.0 mM, $CBPQT^{4+}$ 2.0 mM. [i] The binding constant for the inclusion complex between diethyleneglycol-disubstituted TTF and $CBPQT^{4+}$ was determined to be 380.0×10^3 M^{-1} in MeCN by ITC.[24] [j] The binding constant for the inclusion complex between triethyleneglycol-disubstituted BZ and $CBPQT^{4+}$ was determined to be 1100 M^{-1} in MeCN by UV/Vis titration.[25] [k] The binding constant for the inclusion complex between diethyleneglycol-disubstituted DNP and $CBPQT^{4+}$ was determined to be 36.4×10^3 M^{-1} in MeCN by ITC.[24]

almost all of the $CBPQT^{4+}$ rings reside on only the TTF station. The relative populations are wholly consistent with the absorption spectra of **1**·4PF_6 and **2**·4PF_6 (Figure 5).

^{1}H NMR Spectroscopic Analysis of the Three-Station [2]Catenanes

The ^{1}H NMR spectra of **1**·4PF_6 and **2**·4PF_6 are shown in Figure 6. Interestingly, the spectra of these two three-station [2]catenanes are completely different from each other, despite the fact that their molecular structures are so similar. In both cases, a 1:1 correspondence is found between the integrated intensities of the signals arising from the crown ether macrocycles and the $CBPQT^{4+}$ rings, confirming that only one $CBPQT^{4+}$ ring is interlocked with the crown ether macrocycles. The [2]catenane **2**·4PF_6 gives rise to two peaks corresponding to the methylene protons adjacent to the BZ unit ($\delta = 2.97$ and 3.22 ppm; Figure 6b) because of the constitutionally unsymmetrical nature of the crown ether. On the other hand, **1**·4PF_6 affords four peaks for the same CH_2BZ protons ($\delta = 3.00$, 3.08, 3.24, and 3.33 ppm; Figure 6a). All the aromatic protons in the TTF, BZ, and DNP units were assigned by using 2D COSY and NOESY experiments (see Figures S1 and S2 in the Supporting Information). Partial ^{1}H NMR spectra, highlighting the assignment of the protons associated with TTF, BZ, and DNP units in **1**·4PF_6 and **2**·4PF_6, are shown in Figure 7. The number of peaks corresponding to these protons in **1**·4PF_6 (Figure 7a) is twice that observed for **2**·4PF_6 (Figure 7b). The $CBPQT^{4+}$ ring protons in **1**·4PF_6 also give rise to many more peaks than is observed for the $CBPQT^{4+}$ ring in **2**·4PF_6 (Figure 6). The 2D NOESY spectrum of **1**·4PF_6 reveals that there are two sets of four peaks belonging to its $CBPQT^{4+}$ ring. This result indicates that this three-station [2]catenane is comprised of two isomers.

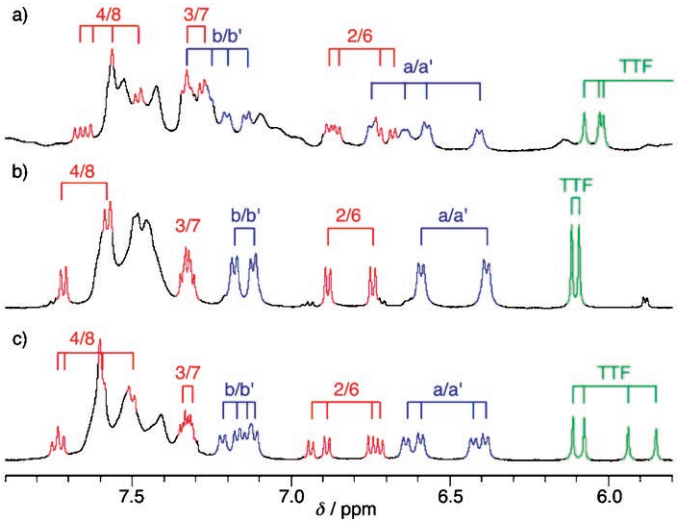

Figure 7. Partial ^{1}H NMR spectra (500 MHz, CD_3CN, room temperature) of a) **1**·4PF_6, b) freshly prepared **2**·4PF_6, and c) **2**·4PF_6 after storing for 5 months. The assignment of the aromatic protons in the TTF, BZ, and DNP stations are shown. The proton descriptions are defined in Figure 2b.

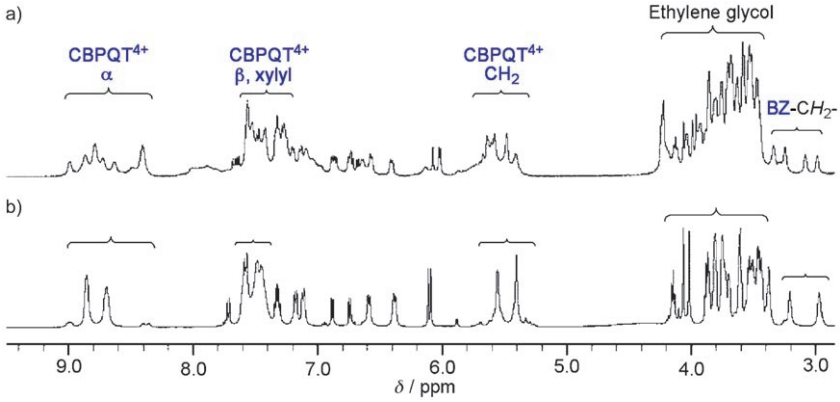

Figure 6. Partial ^{1}H NMR spectra (500 MHz, CD_3CN, room temperature) of a) **1**·4PF_6 and b) **2**·4PF_6. The assignment of the $CBPQT^{4+}$ protons and the methylene protons adjacent to the benzidine unit are shown. The proton descriptions are defined in Figure 2b.

From the relative intensities of the peaks, the molar ratio of the two isomers of **1**·4PF_6 is almost 1:1. The two possible isomers that can be proposed are 1) translational isomers[12a] associated with the partitioning of the $CBPQT^{4+}$ ring between the stations and 2) *cis* and *trans* isomers[12c,d] associated with the TTF unit. Most of the $CBPQT^{4+}$ ring resides on the TTF unit. Thus, we can rule out the former possibility. The

latter, though, is plausible. In the spectrum of **2**·4 PF_6, small peaks were detected, for example, at $\delta = 8.38$ and 8.98 ppm (Figure 6b), that can be associated with the minor isomer. In this case, however, one isomer is predominant. Interestingly, the ratio of the minor to major isomers changes with time in the solution state (Figure 7c). When the sample solution was stored in the dark for five months, the ratio of the two isomers became almost 1:1. A similar phenomenon was observed in our previous studies on two-station TTF-DNP [2]rotaxanes[12c,d] and [2]catenanes,[5e,f] as well as a TTF-containing self-complexing compound. In the TTF-DNP [2]rotaxane, two sets of TTF peaks, associated with the *cis* and *trans* isomers, were reported.[12c,d] On the other hand, it was confirmed that the *trans* isomer of the TTF unit is the predominant one in the TTF-DNP [2]catenane on the basis of ^{1}H NMR spectroscopy and X-ray crystallographic analysis.[5e,f] In the case of the TTF-containing self-complexing compound, one isomer, probably *trans*, becomes predominant[7e] when the sample is stored in the dark for two months. These results imply that the *trans* isomer of TTF becomes predominant when the TTF unit is situated exclusively inside the $CBPQT^{4+}$ ring. Presumably, the *trans* TTF isomer can reside within the $CBPQT^{4+}$ ring more comfortably than the *cis*. The $CBPQT^{4+}$ ring resides exclusively on the TTF unit in the TTF-DNP two-station [2]catenane[5e,f] because the CT interaction between the $CBPQT^{4+}$ and the DNP unit alongside helps to stabilize the complex between the TTF unit and the $CBPQT^{4+}$ ring. In the case of TTF-containing self-complexing compounds, the TTF unit is strongly trapped by the $CBPQT^{4+}$ ring, because no guest comes anywhere near being competitive. The TTF unit in **2**·4 PF_6 is also trapped by the $CBPQT^{4+}$ ring almost exclusively (99.5%; see above), but not perfectly. The imperfect nature of the $CBPQT^{4+}$ ring encapsulation of the TTF unit can lead to a slow change in the equilibrium between the *cis* and *trans* TTF isomers in solution. When the sample was stored in the solid state, no change in the ^{1}H NMR spectrum was observed, even after five months. The situations governing the two-station TTF-DNP [2]rotaxanes[12c,d] and the three-station [2]catenane **1**·4 PF_6 are similar. In both cases, the $CBPQT^{4+}$ ring shuttles between the TTF and DNP units frequently: about 10% of the $CBPQT^{4+}$ rings reside on the DNP unit (see above).[12c,d] In the case of the three-station [2]catenane, the CT interaction between the $CBPQT^{4+}$ ring and the stations alongside is not strong enough for the $CBPQT^{4+}$ ring to reside on the TTF unit exclusively (see below). In this case, we observed a mixture of the *cis* and *trans* TTF isomers. No change in the ^{1}H NMR spectrum was observed when **1**·4 PF_6 was stored in the dark in either solution or the solid state for five months.

Electrochemical Behavior of the Model Compounds

The electrochemical properties of the model guests (TTF-TEG, BZ-TEG, and DNP-TEG), the crown ether **16**, and CBPQT·4 PF_6 were analyzed by cyclic voltammetry (CV) (Figure 8a–d). The results are summarized in Table 2. TTF-TEG shows two typical reversible and monoelectronic oxidation processes (Figure 8a).[5f,10f,13b,15b,31] The observed half-wave potentials for the first and second oxidations (+0.36 and +0.71 V vs. SCE, respectively; a saturated calomel electrode (SCE) was used as the reference electrode in all cases unless otherwise stated) were consistent with previous reports.[5f,10f,13b,15b] BZ-TEG also shows two reversible and monoelectronic processes (Figure 8b).[5d,25] The observed half-wave potentials of the first and second oxidations (+0.46 and +0.65 V, respectively) of BZ-TEG were 0.07 V less than the previously reported values (+0.53 and +0.71 V vs. Ag/AgCl). These differences in potential may arise from the use of different reference electrodes. Herein, we used an SCE electrode as the reference whereas pre-

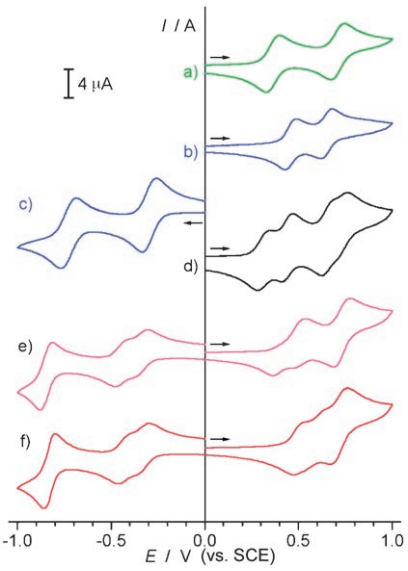

Figure 8. Cyclic voltammograms of a) the TTF model compound TTF-TEG, b) the BZ model compound BZ-TEG, c) the cyclophane CBPQT·4 PF_6, d) the crown ether **16**, and the three-station [2]catenanes e) **1**·4 PF_6 and f) **2**·4 PF_6. All data were recorded at 200 mV s^{-1} in argon-purged MeCN at room temperature. The 5.0×10^{-4} mol L^{-1} sample solutions were prepared by using a 0.1 mol L^{-1} solution of TBA·PF_6 (TBA = tetra-*n*-butylammonium). The working electrode was a glassy carbon electrode (0.0178 cm^2).

Table 2. Electrochemical data for the model compounds.[a]

Compound	Half-wave potentials versus SCE [V]	
	Oxidation[b]	Reduction[b]
TTF-TEG	+0.36, +0.71	–
BZ-TEG	+0.46, +0.65	–
DNP-TEG	+1.16[c]	–
16	+0.31[d], +0.44[d], +0.65[d], +0.71[d], +1.37[c,d]	–
$CBPQT^{4+}$·4 PF_6	–	−0.29[e], −0.72[e]

[a] Argon-purged MeCN, room temperature, 0.1 M TBA·PF_6 as supporting electrolyte, glassy carbon as working electrode. The sample concentration was 0.5 mM. [b] Reversible and monoelectronic processes, unless otherwise indicated. [c] Quasireversible process. [d] Overlapping CV peaks; half-wave potentials were determined by DPV peaks. [e] Two-electron reversible process.

viously[5d,25] an Ag/AgCl electrode was employed. The first-oxidation potential (+1.16 V) of DNP-TEG is much larger[5f,13b] than those of TTF-TEG and BZ-TEG. Although the redox behavior of the macrocycle **16** is almost the sum of that of TTF-TEG and BZ-TEG, the first-oxidation potentials of the TTF and BZ units in **16** (Figure 8d) are less positive than those of TTF-TEG and BZ-TEG. Notably, the first-oxidation potential of the TTF unit in the crown ether is 50 mV less positive than that of TTF-TEG. This result can be accounted for by the π–π stacking interaction between the TTF and DNP units, as was previously observed for other crown ether derivatives.[5f,32] The oxidation potential of the DNP unit in **16** is displaced 210 mV toward a more-positive value relative to that of DNP-TEG (Table 2). This large displacement points to a CT interaction between the π-electron-rich DNP unit and the π-electron-deficient doubly oxidized TTF and BZ units.[5f] When we set the potential scan range from 0.0 to +1.0 V, the CV traces for the second, third, and fourth successive scans for the crown ether were identical. However, the cathodic peaks of the BZ unit disappeared when we scanned up to +1.5 V; only the redox peaks of the TTF and DNP units were observable in the successive scans. This result indicates that the BZ unit suffers an irreversible transformation at the higher applied potentials (+1.0 to +1.5 V) and loses its electroactive properties. The tetracationic cyclophane salt CBPQT·4 PF_6 shows the two typical reversible and two-electron reduction processes (Figure 8c),[5f,12d,15b,32a,33] the half-wave potentials of which are consistent with the previously reported values of −0.29 and −0.72 V.[5f,12d,15b,32a,33]

Electrochemical Behavior of the Three-Station [2]Catenanes

The CV traces of **1**·4 PF_6 and **2**·4 PF_6 are shown in Figure 8e and f, respectively, and their dependence on scan rate is recorded in Figure 9. In the case of these [2]catenanes, some of the redox potentials are different when comparing anodic and cathodic scans. The half-wave potentials of the redox processes were determined by DPV analysis (Figure 10) and are summarized in Table 3. In the reduction part of the CV, the well-known splitting[5a,32,33] of the first two-electron reduction peaks and the displacement of all the processes to more-negative potentials were observed. These processes (**1**·4 PF_6: −0.31, −0.43, −0.82 V; **2**·4 PF_6: −0.30, −0.41, −0.80 V) are completely reversible for both [2]catenanes. The splitting of the first two-electron reduction peaks was ascribed[5f,32,33] to the presence of "inside" and "alongside" bipyridinium units. The second one-electron reduction peak was assigned to the "inside" bipyridinium unit of the $CBPQT^{4+}$ ring because the "inside" bipyridinium unit is stabilized by CT interactions[5f,33] with the TTF unit and the other stations. The second one-electron reduction potentials of the TTF-BZ-DNP three-station [2]catenanes **1**·4 PF_6 and **2**·4 PF_6 (−0.43 and −0.41 V, respectively) are much less negative than those for the previously reported TTF-DNP two-station [2]catenane (−0.49 V).[5f] A comparison of this experimental data indicates that the CT interactions between the "inside" bipyridinium unit and the "alongside" stations (BZ and DNP) are small in the three-station [2]catenanes. The larger and unsymmetrical construction of the crown ether in the three-station [2]catenanes presumably militates against the formation of a stable stacked structure similar to that found in the TTF-DNP two-station [2]catenane.[5f] On the other hand, the first one-electron reduction peaks for

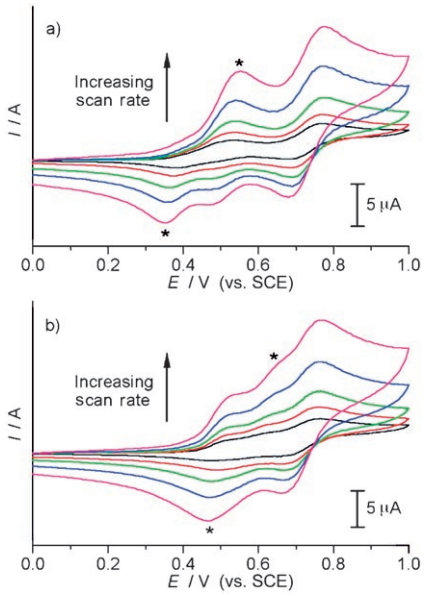

Figure 9. Scan-rate dependence of the cyclic voltammagrams of a) **1**·4 PF_6 and b) **2**·4 PF_6. Scan rates: 50 mV s^{-1} (black), 100 mV s^{-1} (red), 200 mV s^{-1} (green), 400 mV s^{-1} (blue), 800 mV s^{-1} (purple). All data presented were recorded at 200 mV s^{-1} in argon-purged MeCN at room temperature.

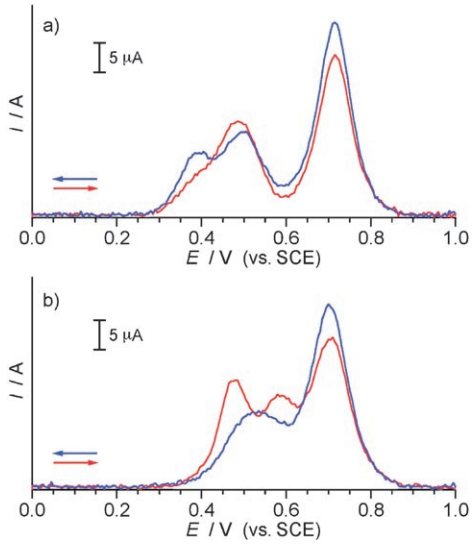

Figure 10. Differential pulse voltammetry (DPV) peaks of a) **1**·4 PF_6 and b) **2**·4 PF_6. Both data were recorded in argon-purged MeCN at room temperature. The 5.0×10^{-4} mol L^{-1} sample solutions were prepared by using a 0.1 mol L^{-1} solution of TBA·PF_6. The working electrode was a glassy carbon electrode (0.0178 cm^2). The red and blue traces represent the data recorded in the anodic and cathodic scans, respectively.

Table 3. DPV peak potentials versus SCE (V) for **1**·4PF_6 and **2**·4PF_6.[a]

Compound	Scan direction	Oxidation[b]	Reduction[b]
1·4PF_6	Anodic	+0.39, +0.49, +0.71[c]	−0.32, −0.44, −0.83[d]
	Cathodic	+0.38, +0.49, +0.71[c]	−0.32, −0.44, −0.84[d]
2·4PF_6	Anodic	+0.48, +0.58, +0.70[c]	−0.31, −0.42, −0.81[d]
	Cathodic	+0.53,[c] +0.70[c]	−0.32, −0.42, −0.81[d]

[a] Argon-purged MeCN, room temperature, 0.1 mol L^{-1} TBA·PF_6 as supporting electrolyte, glassy carbon as working electrode. Sample concentration: 5.0×10^{-4} M. [b] Peak potential values determined by using the curve-fitting operation of the IGOR Pro software (Version 5.04B, WaveMetrix, Inc.). The relation between the peak potential in the DPV measurement (E_{max}), half-wave potential ($E_{1/2}$), and pulse height (ΔE) is $E_{1/2}=E_{max}+\Delta E/2$.[35] In this study, ΔE was set to 25 mV. [c] Two inseparable one-electron processes. [d] Two-electron process.

1·4PF_6 and **2**·PF_6 (−0.31 and −0.30 V, respectively) are slightly more positive than for the TTF-DNP two-station [2]catenane (−0.33 V).[5f] A comparison of this experimental data indicates that the electrochemical environments of the "alongside" bipyridinium units in the two- and three-station [2]catenanes are very similar. The two-electron reduction potentials of **1**·4PF_6 and **2**·PF_6 (−0.82 and −0.80 V, respectively) are much less negative than that for the TTF-DNP two-station [2]catenane (−0.87 V).[5f] The larger crown ether in the three-station [2]catenane relative to that in the two-station catenane probably results in a smaller CT interaction between the crown ether and the $CBPQT^{4+}$ ring.

Although the electroactive units (TTF, BZ, and DNP) in the macrocycle **16** and the [2]catenanes **1**·4PF_6 and **2**·PF_6 are the same, the CV traces (Figure 8d–f, respectively) in the oxidation region are very different from each other. Two distinct CV peaks (+0.54 and +0.78 V) were detected in the anodic scan of **1**·4PF_6; from the peak intensities, each peak corresponds to a two-electron process. DPV measurements clarified that the first anodic CV peak (+0.54 V) in **1**·4PF_6 consists of two overlapping peaks (Figure 10a, red trace). The DPV peak potentials in the anodic scan were found to be +0.39, +0.49, and +0.71 V. The DPV peak at +0.39 V is distinctively small; indeed, it is a shoulder on the peak at +0.49 V. In the cathodic scan of **1**·4PF_6, three distinct peaks (+0.36, +0.47, and +0.69 V) can be seen in the CV trace. DPV measurements also show three distinct peaks (Figure 10a, blue trace). The DPV peak potentials in the cathodic scan were found to be +0.38, +0.49, and +0.71 V. The DPV peak intensities at +0.38 and +0.49 V are almost the same. By taking both the CV and DPV peak intensities into account, the DPV peaks at +0.38, +0.49, and +0.71 V are considered to be one-, one-, and two-electron processes, respectively. Figure 8a shows the scan-rate dependency of the CV traces for **1**·4PF_6. On increasing the scan rate, the anodic CV peak at around +0.54 V moves toward more-positive potentials, and the cathodic CV peak at around +0.36 V toward less-positive potentials. The other redox peaks are almost independent of the scan rate. The scan-rate dependency of the CV peaks implies that these redox reactions are accompanied by movement of the mechanically interlocked $CBPQT^{4+}$ ring.[5f] The details of the CV and DPV peak assignments are discussed later along with the spectroelectrochemical results.

In the case of **2**·4PF_6, three distinct CV peaks (+0.54, +0.64, and +0.75 V) were detected in the anodic scan. The DPV analysis also showed three distinct peaks at +0.48, +0.58, and +0.70 V. The CV and DPV peak intensities suggest that the first of the two peaks correspond to one-electron processes, whereas the last peak corresponds to a two-electron process. In the cathodic scan of **2**·4PF_6, two distinct peaks (+0.47 and +0.67 V) were detected. Even in the DPV analysis, only two peaks were observed (Figure 10b, blue trace) at +0.53 and +0.70 V. Each of these two peaks is considered to be a two-electron process. It was confirmed that the anodic CV peak at +0.64 V and cathodic peak at +0.47 V showed scan-rate dependency (Figure 9b). These redox reactions are believed to take place along with the rearrangement of the interlocked $CBPQT^{4+}$ ring.

We recorded four successive CV scans (scan range: −1.0→+1.0 V) for **1**·4PF_6 and **2**·4PF_6. In both cases, the second, third, and fourth CV scans were identical. Furthermore, we confirmed that the CV peak intensity, determined from the second two-electron oxidation peaks, obeys the square-root power of the scan rate in the range 50–800 mV s^{-1}. These results indicate that the three-station [2]catenanes suffered no damage under these experimental conditions. If the potential was scanned up to +1.5 V, however, the peaks corresponding to the BZ redox reactions disappeared in subsequent scans.

Spectroelectrochemistry of the [2]Catenanes

Figure 11 illustrates the results of UV/Vis spectroelectrochemistry (SEC) for the three-station [2]catenanes **1**·4PF_6 and **2**·4PF_6. In these experiments, UV/Vis spectra were recorded while scanning the applied voltage on the sample electrolyte solution. The change in the spectra in response to the applied voltage is useful for elucidating the electrochemical processes with many electroactive species.[10f] To assign the absorption bands, the electrochemical measurements were performed for the model compounds TTF-TEG and BZ-TEG. The results are summarized in Table 4.

At the ground state ($E=0$ mV), the UV/Vis spectra of **1**·4PF_6 display a characteristic band at 835 nm assigned to the TTF→$CBPQT^{4+}$ electronic transition.[5e,f,10f,12c,15b] The characteristic absorption bands ($\lambda_{max}=445$ and 595 nm) assigned to the $TTF^{\cdot+}$ radical cation[5e,f,10f,12c,15b,31] emerged in the potential range 320–600 mV. At the same time, the intensity of the CT band ($\lambda_{max}=835$ nm) decreased ($E=$ 600 mV in Figure 11). This result indicates that the first oxidation of **1**·4PF_6 occurs at the TTF unit and that the $CBPQT^{4+}$ ring circumrotates away from the TTF to the other stations.[5,10f,12] As shown by the association constants of CBPQT·4PF_6 and the model compounds BZ-TEG and DNP-TEG, the $CBPQT^{4+}$ ring resides preferentially on the DNP unit after the oxidation of the TTF unit. In the potential range 600–840 mV, the characteristic absorption bands ($\lambda_{max}=460$ and 835 nm) assigned to the $BZ^{\cdot+}$ radical cation

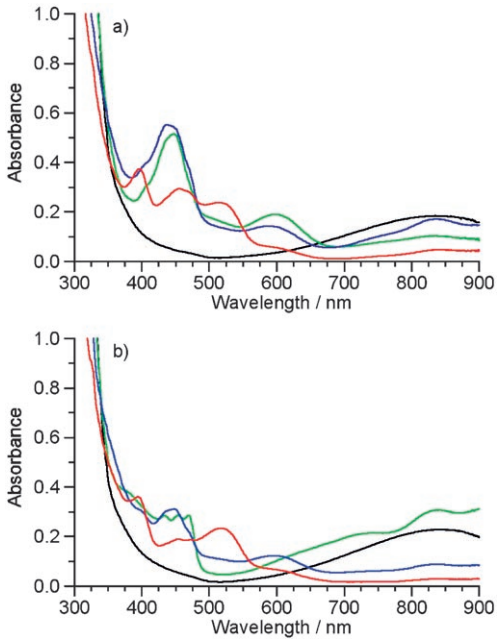

Figure 11. UV/Vis spectroelectrochemistry of a) **1**·4PF$_6$ and b) **2**·4PF$_6$. The UV/Vis spectra were recorded while scanning the potential applied to the electrolyte solution (scan rate: 0.25 mV s^{-1}). Both data were recorded in argon-purged MeCN at room temperature. The 5.0×10^{-4} mol L^{-1} sample solutions were prepared by using a 0.1 mol L^{-1} solution of TBA·PF$_6$. The working, counter, and reference electrodes were the Pt grid, Pt coil, and Ag wire, respectively. $E=0$ (——), 600 (——), 840 (——), 1020 mV (——).

Table 4. UV/Vis spectroscopic properties of the TTF and BZ radical cation and dication.[a]

Compound	Absorption band [nm]	λ_{max} [nm]
TTF·$^+$[b]	380–680	445, 595
TTF^{2+}[b]	440–580	515
BZ·$^+$[c]	350–480	380, 460
	580–>900	660, 835
BZ^{2+}[c]	380–500	460

[a] All the data were obtained by SEC measurements. UV/Vis spectra were recorded by scanning the potential applied to the electrolyte solution (scan rate: 0.5 mV s^{-1}) at room temperature. Concentration of the sample: 5.0×10^{-4} mol L^{-1}, concentration of the supporting electrolyte TBA·PF$_6$: 0.1 mol L^{-1}, solvent: argon-purged MeCN, working electrode: Pt grid, counter electrode: Pt coil, reference electrode: Ag wire. [b] Data for the TTF radical cation and dication were obtained by using TTF-TEG as a model compound. [c] Data for BZ radical cation and dication were obtained by using BZ-TEG as a model compound.

were detected ($E=840$ mV in Figure 11a). In the potential range 840–1020 mV, the spectra displayed a partial bleaching of the TTF·$^+$ ($\lambda_{max}=445$ and 595 nm) as well as the BZ·$^+$ radical-cation bands ($\lambda_{max}=835$ nm), with the formation of new peaks assigned to the TTF^{2+} ($\lambda_{max}=515$ nm) and BZ^{2+} ($\lambda_{max}=460$ nm) dications. Notably, the changes in the UV/Vis spectra do not correlate directly with the expected results from the oxidation potentials determined by DPV analysis. In this SEC analysis, we scanned the applied potential slowly and continuously without checking whether the system could reach electrochemical equilibrium. As it takes some time to oxidize enough molecules to effect a change in the UV/Vis spectrum, the effect of one applied potential appears as spectral changes at a higher potential. This time lag between cause and effect results in the displacement between the half-wave potential and the applied voltage in the SEC. We attempted to hold the potential at a constant value until electrochemical equilibrium was reached. However, the irreversible reaction of the BZ·$^+$ radical cation took place and precipitation of a black product occurred, reflecting the polymerization of the benzidine.[34] Although the relationship between the applied potential and the UV/Vis spectrum is ambiguous in this SEC experiment, the sequence of the oxidation processes is reliable enough for the assignment of the CV and DPV peaks. The first and second oxidation peaks in DPV ($E=+0.39$ and $+0.49$ V) were assigned to the first oxidations of the TTF and BZ units, respectively, and the third DPV peak at $+0.71$ V corresponds to the oxidations of the TTF·$^+$ and BZ·$^+$ radical cations. The details of the electromechanical properties will be discussed in the following section.

Let us now consider the SEC of **2**·4PF$_6$. In the ground state ($E=0$ mV), **2**·4PF$_6$ also shows the TTF→CBPQT^{4+} CT band at 840 nm.[5e,f,10f,12c,15b] In the potential range 480–600 mV, we confirmed the emergence of the characteristic absorption bands ($\lambda_{max}=460$ and 835 nm) for the BZ·$^+$ radical cation. Thus, in the case of this [2]catenane, the first oxidation takes place at the BZ unit. The absorption intensity around 800 nm is the sum of the TTF→CBPQT^{4+} CT band and the absorption of the BZ·$^+$ radical cation, indicating that the formation of BZ·$^+$ should not affect the location of the CBPQT^{4+} ring. In the potential range 600–840 mV, absorption bands assigned[5e,f,10f,12c,15b,31] to the TTF·$^+$ radical cation ($\lambda_{max}=445$ and 595 nm) were detected. This change in the spectrum was accompanied by bleaching of the TTF→CBPQT^{4+} CT band, indicating that the first oxidation of TTF and the rearrangement of the CBPQT^{4+} ring takes place in this potential range. As the BZ unit is already oxidized, the CBPQT^{4+} ring should move to the DNP unit after the oxidation of the TTF unit. In the potential range 840–1020 mV, the spectra displayed a partial bleaching of the TTF·$^+$ ($\lambda_{max}=445$ and 595 nm) and BZ·$^+$ radical-cation bands ($\lambda_{max}=835$ nm), with the formation of new peaks assigned to the TTF^{2+} ($\lambda_{max}=515$ nm) and BZ^{2+} ($\lambda_{max}=460$ nm) dications. The intensity of the BZ^{2+} absorption in **2**·4PF$_6$ at $+1020$ V is smaller than that observed in the case of **1**·4PF$_6$. As the BZ unit in **2**·4PF$_6$ is oxidized at an earlier stage than that in **1**·4PF$_6$, the BZ·$^+$ radical cation in **2**·4PF$_6$ suffers more-serious damage when oxidized to BZ^{2+} than it does in **1**·4PF$_6$. The propensity of BZ·$^+$ to polymerize accounts for the lower intensity of the BZ^{2+} absorption band in the case of **2**·4PF$_6$.

SEC measurements revealed clearly that in **1**·4PF$_6$ and **2**·4PF$_6$, the first oxidation occurs at the TTF and BZ units, respectively. The DPV peaks associated with the first oxidations of BZ occur at almost the same potentials in **1**·4PF$_6$

and **2**·4PF$_6$ (+0.49 and +0.48 V, respectively). The oxidation sequence of the TTF, BZ, and DNP units depends on whether the first-oxidation potential of the TTF unit is higher or lower than that of the BZ unit. As the complexation between the CBPQT^{4+} ring and the π-electron-rich competitive recognition sites is an equilibrium process, **1**·4PF$_6$ contains a small amount (<10%) of "free" TTF even in the initial state. This phenomenon rationalizes the different oxidation sequences in the two three-station [2]catenanes.

In the case of **1**·4PF$_6$, about 10% of the CBPQT^{4+} ring reside on the DNP stations (see above). The small shoulder DPV peak at +0.39 V for this [2]catenane (Figure 10a, red trace) most likely corresponds to the oxidation of the uncomplexed TTF unit. The low intensity of this DPV peak arises from the fact that the "free" TTF units are a minor species at equilibrium. In the cathodic scan of the DPV, by comparison with the half-wave potential of the model compound TTF-TEG, the peak at +0.38 V is assigned to the reduction of the TTF$^{\cdot+}$ radical cation. The reduction potential of TTF$^{\cdot+}$ in the [2]rotaxane is not affected by the CBPQT^{4+} ring[5,10,12] because this ring is on the other station when TTF is in its oxidized form. This result also supports the fact that the DPV peak at +0.39 V in the anodic scan corresponds to the oxidation of the "free" TTF unit. The DPV peak for the first oxidation of the occupied TTF unit probably overlaps with the peak for the first BZ oxidation at +0.49 V. On the other hand, the first oxidation of TTF in **2**·4PF$_6$ occurs at +0.58 V. In the case of this [2]catenane, 99.5% of the CBPQT^{4+} rings reside on the TTF unit (see above). The CBPQT^{4+} ring in **2**·4PF$_6$ shuttles between the stations much less frequently than it does in **1**·4PF$_6$. As a result, the first oxidation of the TTF unit in **2**·4PF$_6$ is displaced to a much more positive potential than that in **1**·4PF$_6$. In our previous investigations on TTF-DNP two-station [2]catenanes,[5e,f] the first-oxidation potential of the TTF unit was found to overlap with the second oxidation peak at +0.76 V. In relation to this previous finding,[5f] the TTF unit in the three-station [2]catenane is oxidized more easily. In the case of the TTF-DNP two-station [2]catenane,[5e,f] the π–π stacking between the CBPQT^{4+} ring and the "alongside" DNP unit enhances the stability of the translational isomer in which the CBPQT^{4+} ring encircles the TTF unit, ensuring that the oxidation of the TTF unit is strongly inhibited. On the other hand, the π–π stacking between the CBPQT^{4+} ring and the "alongside" BZ and DNP units is less stabilizing in the three-station [2]catenane **2**·4PF$_6$. This same line of reasoning has already been used (see above) in the discussion of the reduction potentials of the CBPQT^{4+} ring.

Electromechanical Behavior of [2]Catenanes

In this section, we discuss the electromechanical behavior of **1**·4PF$_6$ and **2**·4PF$_6$ based on the results of the ITC, CV, DPV, and SEC measurements. Scheme 4 shows the proposed electromechanical behavior of **1**·4PF$_6$. In its ground state, the CT band in the UV/Vis spectrum indicates that the CBPQT^{4+} ring is located on the TTF unit [state (i)].[5e,f,10f,12c,15b,21] ITC results, however, suggest that an equilibrium exists between state (i) and (i′). We estimated that about 10% of the CBPQT^{4+} ring encircles the DNP unit, based on thermodynamic comparisons with model compounds. The TTF unit in state (i′) is easily oxidized to the TTF$^{\cdot+}$ radical cation. The small shoulder DPV peak at +0.39 V most likely corresponds to this process [(i′)→(ii), red arrows]. The oxidation of the occupied TTF and BZ units takes place at almost the same potential, that is, around +0.50 V [(i)→(ii)→(iii), red arrows]. The oxidative

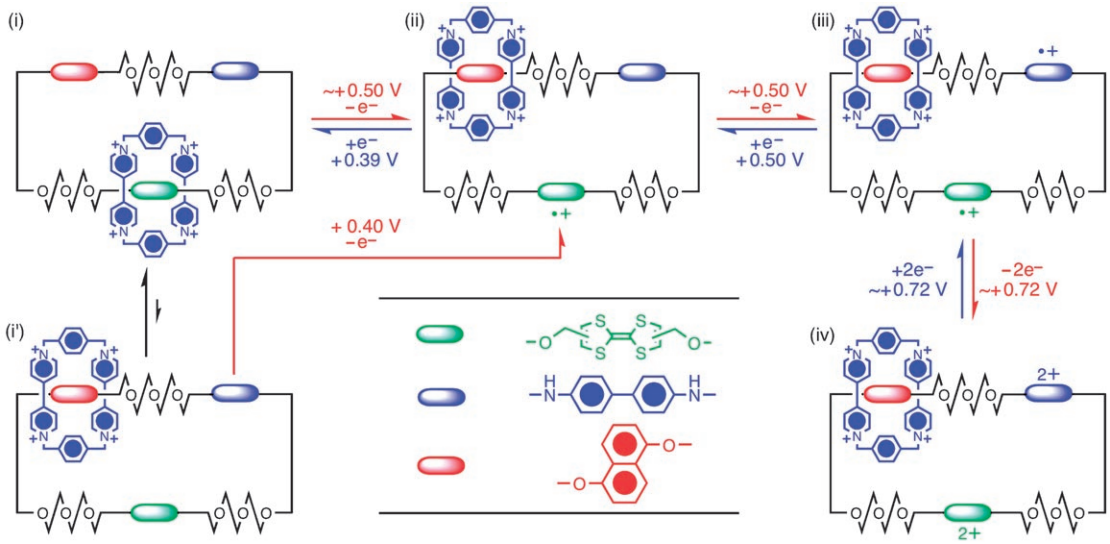

Scheme 4. Proposed electromechanical behavior of **1**·4PF$_6$. In the ground state, **1**·4PF$_6$ is in equilibrium between states (i) and (i′). The red and blue arrows represent the oxidation and reduction processes, respectively. The half-wave potentials determined from the DPV analysis are depicted by the arrows.

process involving the TTF unit is accompanied by the circumrotation of the $CBPQT^{4+}$ ring because of the electrostatic repulsive force between $CBPQT^{4+}$ and $TTF^{\cdot+}$.[5,10,12,21] As shown by the relatively large K_a value of the DNP unit relative to the BZ unit towards $CBPQT{\cdot}4PF_6$, the $CBPQT^{4+}$ ring remains preferentially on the DNP unit in state (ii). The further oxidation of the $TTF^{\cdot+}$ and $BZ^{\cdot+}$ radical cations takes place at almost the same potential, that is, around +0.72 V [(iii)→(iv), red arrows]. This process is reversible. The TTF^{2+} and BZ^{2+} dications are reduced to their corresponding radical cations at around +0.72 V [(iv)→(iii), blue arrow]. The reduction of $BZ^{\cdot+}$ occurs at +0.50 V [(iii)→(ii), blue arrows]. The reduction of $TTF^{\cdot+}$ then takes place at +0.39 V [(ii)→(i), blue arrows]. As the $CBPQT^{4+}$ ring encircles the DNP unit in the reduction process, the reduction potential of $TTF^{\cdot+}$ is not affected to any extent by the CT interaction with the $CBPQT^{4+}$ ring.[5,10,12,21] As a result, the reduction potential of $TTF^{\cdot+}$ is close to the oxidation potential of "free" TTF [(i′)→(ii)]. Overall, we cannot determine a state in which the $CBPQT^{4+}$ ring resides preferentially on the BZ unit. As a consequence, we conclude that the three-station catenane $\mathbf{1}{\cdot}4PF_6$ is actually a bistable entity.

Scheme 5 illustrates the proposed electromechanical behavior of the three-station [2]catenane $\mathbf{2}{\cdot}4PF_6$. The CT band ($TTF \rightarrow CBPQT^{4+}$) in the UV/Vis spectrum and the thermodynamic data suggest that the $CBPQT^{4+}$ ring resides on the TTF unit almost exclusively in $\mathbf{2}{\cdot}4PF_6$ [state (i)]. The first oxidation takes place at the BZ unit at +0.49 V [(i)→(ii), red arrow]. In the SEC experiment, the CT band ($TTF \rightarrow CBPQT^{4+}$) was not bleached in this process, indicating that this first oxidation of the BZ unit does not affect the location of $CBPQT^{4+}$. The first oxidation of the TTF unit then occurs at +0.59 V accompanied by the circumrotation of the $CBPQT^{4+}$ ring [(ii)→(iii), red arrow].[5,10,12,21] As the BZ unit has already been oxidized to the radical cation at this potential, the $CBPQT^{4+}$ ring is obliged to move to the DNP station. Further oxidation of the $TTF^{\cdot+}$ and $BZ^{\cdot+}$ radical cations takes place at almost the same potential of around +0.71 V [(iii)→(iv), red arrow]. These redox processes are reversible. The TTF^{2+} and BZ^{2+} dications return to the corresponding radical cations at around +0.71 V [(iv)→(iii), blue arrow]. The broad inseparable DPV peak at +0.53 V indicates that the reductions of $TTF^{\cdot+}$ and $BZ^{\cdot+}$ take place at similar potentials. In some molecules, the reduction of the $BZ^{\cdot+}$ occurs before $TTF^{\cdot+}$. In such cases, the $CBPQT^{4+}$ ring resides preferentially on the neutral BZ unit, that is, the reduction process goes from state (iii) to state (i) via state (ii′). Other molecules undergo another route through state (ii). By means of this route, the reduction of $TTF^{\cdot+}$ and the circumrotation of $CBPQT^{4+}$ to the TTF unit occur before the reduction of $BZ^{\cdot+}$. We have no experimental evidence to indicate which route is the major. Some molecules, however, presumably go through state (ii′). We are, therefore, led to the conclusion that three-station [2]catenane $\mathbf{2}{\cdot}4PF_6$ is a quasi-tristable [2]catenane.

Conclusions

There is no doubt that the substitution of the ether oxygen atoms around the DNP unit with methylene groups is very effective in decreasing the binding ability of the DNP unit

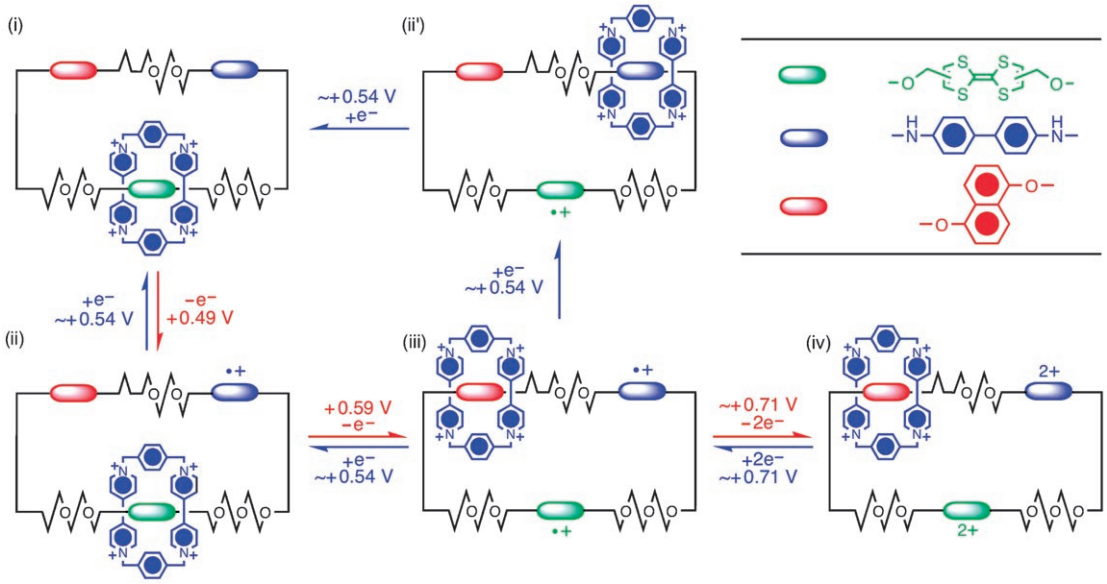

Scheme 5. Proposed electromechanical behavior of $\mathbf{2}{\cdot}4PF_6$. The red and blue arrows represent the oxidation and reduction processes, respectively. The half-wave potentials determined from the DPV analysis are depicted with the arrows. As the reduction potentials of the $TTF^{\cdot+}$ and $BZ^{\cdot+}$ radical cations are almost the same, two reduction processes can be proposed: (iii)→(ii)→(i) and (iii)→(ii′)→(i). In the latter case, the $CBPQT^{4+}$ ring goes through all of the three stations.

for the $CBPQT^{4+}$ ring. Using this modification of chemical structure, we obtained consistency in the orders of magnitude of the binding constants [K_a(TTF-TEG) > K_a(BZ-TEG) > K_a(DNP-C_5-TEG)] and those of the half-wave potentials [$E_{1/2}$(TTF-TEG) < $E_{1/2}$(BZ-TEG) < $E_{1/2}$(DNP-TEG)] in the model compounds. In the three-station [2]catenane **2**·4PF_6, however, the first oxidation took place at a BZ unit as a result of the influence of the $CBPQT^{4+}$ ring upon the oxidation potential of TTF. Although we could not demonstrate the tristability in the oxidation of **2**·4PF_6, some of the $CBPQT^{4+}$ rings reside on the BZ station during the reduction process involving the $TTF^{\cdot+}$ and $BZ^{\cdot+}$ radical cations. Thus, we can describe **2**·4PF_6 as a quasi-tristable system. The findings reported herein are undoubtedly important in demonstrating electrochemically controllable tristable [2]catenanes. Indeed, we can derive some assistance from the results to date for future designs of three-station [2]catenanes. For instance, we should employ the station with the higher oxidation potential (not BZ) to induce the first oxidation at the TTF station. To decrease the oxidation potential of the TTF station encircled by the $CBPQT^{4+}$ ring, we should use a station with a higher binding affinity than BZ. Furthermore, the absorption bands of the oxidized TTF and BZ units may screen weaker CT bands that arise from the interactions between the $CBPQT^{4+}$ ring and each of the three stations. This problem is one that we believe can be solved in the fullness of time. In both TTF-DNP two-station [2]catenanes and [2]rotaxanes, we ascertained previously that the metastable state, in which the $CBPQT^{4+}$ ring encircles the DNP unit when the TTF unit is neutral, displays a red color arising from the DNP→$CBPQT^{4+}$ CT interaction.[21] In a device environment, we found that the relaxation of the metastable state back to the ground state is much slower (≈2000 times) than that in the solution phase,[24] a phenomenon that allows us, in principle, to detect the weaker CT bands clearly. In practice, it would mean introducing impediments to the circumrotation of the macrocyclic polyether ring through the middle of the $CBPQT^{4+}$ ring. We are just starting a journey of exploration of the design features of electrochemically controllable tristable [2]catenanes. Such a journey will ultimately lead to developments that will herald the application of mechanically interlocked molecules to the field of nanoelectromechanical systems.

Experimental Section

General Methods

All chemicals except for 5-bromo-1-pentanol, which was obtained from TCI, were purchased from Aldrich and used as received, unless otherwise indicated. Compounds **7**·2PF_6,[33] **9**,[27] **13**,[27] **18**[13a], and TTF-OH[28] were all prepared according to literature procedures. High-pressure experiments were carried out in a teflon tube on a Psika high-pressure apparatus. Thin-layer chromatography (TLC) was performed by using aluminum sheets precoated with silica gel 60F (Merck 5554). The plates were inspected under UV light. Column chromatography was carried out with silica gel 60F (Merck 9385, 0.040–0.063 mm). ^{1}H NMR spectra were recorded at room temperature on a Bruker ARX500 (500 MHz) or a Bruker ARX400 spectrometer (400 MHz) with residual solvent as the internal standard. ^{13}C NMR spectra were recorded at room temperature on a Bruker ARX500 (125 MHz) or a Bruker ARX400 spectrometer (100 MHz) with residual solvent as the internal standard. All chemical shifts are quoted on a δ scale, and all coupling constants (J) are expressed in Hertz (Hz). The following abbreviations are used in listing the NMR spectra: s = singlet, d = doublet, t = triplet, q = quartet, br = broad, and m = multiplet. Samples were prepared in $CDCl_3$ or CD_3CN purchased from Cambridge Isotope Labs. Electrospray mass spectra (ESI MS) were recorded on a VG ProSpec triple-focusing mass spectrometer. UV/Vis spectra were recorded at room temperature on a Varian Cary 100 Bio UV/Vis spectrophotometer. Electrochemical and spectroelectrochemical experiments were carried out at room temperature in argon-purged MeCN, with a Princeton Applied Research 263A Multipurpose instrument interfaced to a PC. CV experiments were performed by using a glassy carbon working electrode (0.018 cm^2, Cypress Systems); its surface was polished routinely with a 0.05-μm alumina/water slurry on a felt surface immediately before use. The counter electrode was a Pt wire and the reference electrode was an SCE. $TBAPF_6$ (0.1 M) was added as supporting electrolyte. For reversible processes, half-wave potentials ($E_{1/2}$) were calculated from an average of the cathodic and anodic CV peaks.[35] To establish the reversibility of a process,[35] the criteria of 1) 60 mV between cathodic and anodic peaks and 2) close-to-unity ratio of the intensities of the cathodic and anodic currents were employed. As for the irreversible process, $E_{1/2}$ was calculated[35] from the DPV peak top (E_{max}) and pulse height (ΔE) by using the equation of $E_{1/2} = E_{max} + \Delta E/2$. ΔE was set to 25 mV. The E_{max} values for the overlapping peaks were determined by using the curve-fitting operation of the IGOR Pro software (Version 5.04B, Wavemetrix, Inc.). Spectroelectrochemical experiments were made in a custom-built optically transparent thin-layer electrochemical (OTTLE) cell with an optical path of 1 mm, using a Pt grid as working electrode, a Pt wire as counter electrode and a Ag wire pseudoreference electrode. Experimental errors: potential values, ±10 mV; absorption maxima, ±2 nm.

10: Monotosylate **9** (18.0 g, 51.7 mmol), BZ (4.0 g, 21.7 mmol), and Et_3N (20 mL) were dissolved in PhMe (100 mL). The reaction mixture was heated under reflux in the dark for 24 h. After cooling to room temperature, the solvent was removed by evaporation. The residue was dissolved in CH_2Cl_2 (200 mL), washed with saturated aqueous $NaHCO_3$ (200 mL), and dried ($MgSO_4$). After filtration and evaporation, the residue was subjected to column chromatography (SiO_2). The benzidine and monosubstituted benzidine derivative were removed (CH_2Cl_2/Me_2CO = 2:1). Then, the disubstituted benzidine derivative was recovered (CH_2Cl_2/Me_2CO = 1:2), and the solvent was evaporated to give **10** (5.7 g, 49 %) as a dark-orange oil. ^{1}H NMR (400 MHz, $CDCl_3$): δ = 3.09 (br, 2H), 3.31 (t, 4H), 3.57–3.73 (m, 28H), 4.43 (br, 2H), 6.66 (d, J = 8.6 Hz, 4H), 7.33 ppm (d, J = 8.6 Hz, 4H); ^{13}C NMR (100 MHz, $CDCl_3$): δ = 43.7, 61.7, 69.6, 70.2, 70.3, 70.5, 70.7, 72.7, 113.5, 127.0, 130.8, 146.9 ppm; MS (ESI): m/z = 559.3 $[M+Na]^+$.

11: Compound **10** (5.5 g, 10.2 mmol) and di-*tert*-butyl dicarbonate (5.0 g, 22.9 mmol) were dissolved in MeCN (30 mL). The reaction mixture was stirred at room temperature in the dark for 2 days. After the evaporation, the residue was dissolved in CH_2Cl_2 (200 mL), washed with saturated aqueous $NaHCO_3$ (200 mL), dried ($MgSO_4$), filtered, and concentrated to dryness. The residue was purified by column chromatography (SiO_2, EtOAc/Me_2CO = 1:1) to give **11** (6.5 g, 86 %) as an orange oil. ^{1}H NMR (400 MHz, $CDCl_3$): δ = 1.43 (s, 18H), 2.66 (t, 2H), 3.52–3.70 (m, 28H), 3.82 (m, 4H), 7.29 (d, J = 8.2 Hz, 4H), 7.50 ppm (d, J = 8.2 Hz, 4H); ^{13}C NMR (100 MHz, $CDCl_3$): δ = 28.3, 49.4, 61.6, 68.7, 70.2, 70.3, 70.4, 70.6, 72.4, 80.4, 127.0, 127.2, 138.0, 141.9, 154.6, 206.0 ppm; MS (ESI): m/z = 759.4 $[M+Na]^+$.

12: TsCl (1.6 g, 8.4 mmol) dissolved in CH_2Cl_2 (70 mL), was added dropwise over 20–30 min to a solution of **11** (6.0 g, 8.1 mmol), DMAP (55 mg, 0.45 mmol), and Et_3N (1.5 mL, 10 mmol) in CH_2Cl_2 (30 mL). The reaction mixture was stirred for 2 h at room temperature before being diluted with CH_2Cl_2 (150 mL), washed with aqueous HCl (0.1 N, 100 mL), dried ($MgSO_4$), filtered, and concentrated to dryness. The residue was purified

by column chromatography (SiO_2), eluting first of all with the mixed solvent CH_2Cl_2/Me_2CO (4:1) to remove the ditosylate and then with the mixed solvent EtOAc/Me_2CO (1:1) to afford **12** (3.2 g, 44%) as an orange oil. ^{1}H NMR (400 MHz, $CDCl_3$): δ = 1.44 (s, 18H), 2.41 (s, 3H), 2.53 (br, 1H), 3.50–3.70 (m, 26H), 3.82 (m, 4H), 4.11 (m, 2H), 7.25–7.35 (m, 6H), 7.50 (d, J = 8.2 Hz, 4H), 7.77 ppm (d, J = 8.2 Hz, 2H); ^{13}C NMR (100 MHz, $CDCl_3$): δ = 21.6, 28.3, 49.4, 61.6, 68.7, 69.1, 70.2, 70.3, 70.5, 70.6, 72.4, 80.4, 127.0, 127.2, 127.9, 129.7, 132.9, 138.0, 141.9, 144.7, 154.6, 206.3 ppm.

14: Compound **12** (2.5 g, 2.8 mmol), **13** (1.0 g, 3.0 mmol), and K_2CO_3 (0.4 g, 2.9 mmol) were dissolved in MeCN (60 mL). The reaction mixture was heated under reflux for 16 h. After cooling to room temperature, the insoluble material was removed by filtration, and the solvent was evaporated. The residue was dissolved in CH_2Cl_2 (100 mL), washed with aqueous $NaHCO_3$ (100 mL), dried ($MgSO_4$), filtered, and concentrated to dryness. The residue was purified by column chromatography (SiO_2, EtOAc/Me_2CO = 1:1) to afford **14** (2.3 g, 77%) as an orange oil. ^{1}H NMR (400 MHz, $CDCl_3$): δ = 1.44 (s, 18H), 2.53 (br, 2H), 3.52–3.72 (m, 32H), 3.73–3.87 (m, 8H), 3.98 (m, 4H), 4.28 (m, 4H), 6.82 (m, 2H), 7.25–7.35 (m, 6H), 7.50 (d, J = 8.2 Hz, 4H), 7.82 ppm (d, J = 7.5 Hz, 2H); ^{13}C NMR (100 MHz, $CDCl_3$): δ = 28.3, 49.5, 61.7, 67.9, 68.8, 69.8, 70.3, 70.4, 70.5, 70.7, 71.0, 72.5, 80.4, 105.7, 114.6, 125.1, 126.8, 127.1, 127.3, 138.0, 141.9, 154.3, 154.6, 206.4 ppm; MS (ESI): m/z = 1077.6 $[M+Na]^+$.

15: TsCl (0.9 g, 4.5 mmol) dissolved in CH_2Cl_2 (20 mL) was added dropwise over 20–30 min to a solution of **14** (2.0 g, 1.9 mmol), DMAP (12 mg, 9.8×10^{-5} mol), and Et_3N (0.5 mL) in CH_2Cl_2 (20 mL). The reaction mixture was stirred for 4 h at room temperature. The reaction mixture was diluted with CH_2Cl_2 (100 mL), washed with aqueous HCl (0.1N, 100 mL), dried ($MgSO_4$), filtered, and concentrated to dryness. The residue was subjected to column chromatography (SiO_2, EtOAc) to yield **15** (2.3 g, 90%) as a light-yellow oil. ^{1}H NMR (400 MHz, $CDCl_3$): δ = 1.45 (s, 18H), 2.41 (s, 6H), 3.53–3.72 (m, 28H), 3.75–3.88 (m, 8H), 3.98 (m, 4H), 4.12 (m, 4H), 4.28 (m, 4H), 6.82 (d, J = 7.5 Hz, 2H), 7.22–7.32 (m, 10H), 7.50 (d, J = 8.2 Hz, 4H), 7.77 (d, J = 8.0 Hz, 4H), 7.82 ppm (d, J = 7.5 Hz, 2H); ^{13}C NMR (100 MHz, $CDCl_3$): δ = 21.6, 28.3, 49.6, 61.7, 67.9–71.0, 80.4, 105.6, 114.6, 125.1, 126.7, 127.1, 127.3, 128.0, 129.8, 133.0, 138.0, 142.0, 144.8, 154.3, 154.6, 206.4 ppm.

5: TTF-OH (0.26 g, 1.0 mmol) and **15** (1.36 g, 1.0 mmol) dissolved in dry THF (200 mL) were added to a solution of NaH (0.1 g) and Cs_2CO_3 (0.70 g) in dry THF (100 mL) under an atmosphere of dry argon. The reaction mixture was heated under reflux in the dark for 2 days. After cooling to room temperature, the NaH was quenched by a mixed aqueous solution of Me_2CO/H_2O (9:1, 1 mL), and the solid residue was removed by filtration. The solvent was removed by evaporation. The residue was purified by column chromatography (SiO_2, EtOAc) to give **5** (0.37 g, 30%) as a yellow oil. ^{1}H NMR (400 MHz, $CDCl_3$): δ = 1.43 (s, 18H), 3.45–3.71 (m, 32H), 3.72–3.83 (m, 8H), 3.94 (m, 4H), 4.20 (br, 4H), 4.23 (m, 4H), 6.12 (br, 2H), 6.80 (m, 2H), 7.21–7.32 (m, 6H), 7.49 (m, 4H), 7.82 (d, J = 7.5 Hz, 2H); ^{13}C NMR (100 MHz, $CDCl_3$): δ = 28.4, 49.7, 61.7, 68.0–71.0, 80.4, 105.7, 114.6, 116.3, 116.4, 125.1, 126.8, 127.1, 127.4, 128.0, 129.9, 134.4, 134.6, 138.0, 142.0, 154.3, 154.6, 206.2 ppm; MS (ESI): m/z = 1282.5 $[M]^+$.

16: TsOH·H_2O (0.20 g, 1.0 mmol) and **5** (0.15 g, 0.1 mmol) were dissolved in Me_2CO (10 mL). The reaction mixture was heated under reflux in the dark for 2.5 h. After cooling to room temperature, pyridine (0.2 mL) was added. The reaction mixture was subjected to column chromatography (SiO_2, EtOAc) to afford **16** (60 mg, 45%) as a yellow oil. ^{1}H NMR (400 MHz, CD_3CN): δ = 3.18 (t, 2H), 3.28 (t, 2H), 3.50–3.75 (m, 36H), 3.92 (m, 4H), 4.18–4.28 (m, 8H), 4.45 (br, 2H), 6.33–6.34 (m, 2H), 6.56 (m, 2H), 6.64 (m, 2H), 6.92 (m, 2H), 7.21–7.31 (m, 4H), 7.35 (m, 2H), 7.82 ppm (m, 2H); ^{13}C NMR (100 MHz, CD_3CN): δ = 44.7, 68.9, 69.4, 70.4–70.8, 71.3–71.7, 72.0, 107.3, 114.4, 115.5, 118.1, 118.2, 121.3, 126.8, 127.8, 127.9, 131.0, 136.0, 136.1, 148.6, 155.7 ppm; MS (ESI): m/z = 1283.4 $[M+H]^+$.

17: DNP (4.8 g, 30 mmol), 5-bromopentanol (15.0 g, 90 mmol), and K_2CO_3 (12.5 g) were mixed in MeCN (100 mL). The reaction mixture was heated under reflux for 16 h. After cooling to room temperature, the solvent was removed by evaporation. The residue was dissolved in hot $CHCl_3$, and the insoluble material was removed by filtration. After evaporation of the $CHCl_3$, the product was purified by column chromatography (SiO_2, $CHCl_3$/Me_2CO = 4:1). Concentration in vacuo gave **17** (8.0 g, 80%) as a white solid. ^{1}H NMR (400 MHz, $CDCl_3$): δ = 1.41 (br, 2H), 1.60–1.75 (m, 8H), 1.95 (m, 4H), 3.70 (t, 4H), 4.14 (t, 4H), 6.82 (d, J = 7.6 Hz, 2H), 7.35 (t, 2H), 7.84 ppm (d, J = 8.6 Hz, 2H); ^{13}C NMR (100 MHz, $CDCl_3$): δ = 22.9, 29.4, 32.8, 63.2, 68.3, 105.6, 114.4, 125.4, 127.1, 154.9 ppm.

19: Compound **17** (4.0 g, 12.0 mmol), **18** (40.0 g, 0.19 mol), NaI (3.0 g), and NaH (3.5 g) were mixed in dry THF (50 mL). The reaction mixture was heated under reflux for 24 h. After cooling to room temperature, the reaction was quenched with aqueous mixed solvent (Me_2CO/H_2O = 9:1, 10 mL). Then, the solid material and solvent were removed by filtration and evaporation, respectively. The residue was dissolved in $CHCl_3$, filtered, and concentrated to dryness again. The residue was subjected to column chromatography (SiO_2), eluting first with CH_2Cl_2 to remove **18** and then with mixed solvent ($CHCl_3$/Me_2CO = 8:2) to give the product. After evaporation of the solvent, **19** (6.8 g, 83%) was obtained as a colorless oil. ^{1}H NMR (400 MHz, $CDCl_3$): δ = 1.45–1.99 (m, 24H), 3.51 (m, 6H), 3.60 (m, 6H), 3.67 (m, 8H), 3.86 (m, 4H), 4.13 (t, 4H), 4.61 (t, 2H), 6.81 (d, J = 7.6 Hz, 2H), 7.33 (t, 2H), 7.82 ppm (d, J = 8.6 Hz, 2H); ^{13}C NMR (100 MHz, $CDCl_3$): δ = 19.5, 22.9, 25.4, 29.2, 29.5, 30.6, 62.2, 66.7, 68.0, 70.2, 70.5, 70.6 71.3, 98.9, 105.2, 114.1, 125.1, 126.8, 154.6 ppm.

20: Compound **19** (3.4 g, 5.0 mmol) and PPTS (120 mg) were dissolved in a mixed solvent ($CHCl_3$/MeOH = 1:1, 50 mL). The reaction mixture was heated under reflux for 3 h. After cooling to room temperature, the solvent was removed by evaporation. The residue was dissolved in $CHCl_3$ (200 mL), washed with saturated aqueous $NaHCO_3$ (200 mL), dried ($MgSO_4$), and concentrated to dryness. The residue was purified by column chromatography (SiO_2, $CHCl_3$/Me_2CO = 1:1). Concentration in vacuo gave **20** (2.0 g, 80%) as a white solid. ^{1}H NMR (400 MHz, $CDCl_3$): δ = 1.63 (m, 4H), 1.71 (m, 4H), 1.94 (m, 4H), 2.64 (t, 2H), 3.52 (m, 4H), 3.55–3.71(m, 16H), 4.12 (t, 4H), 6.82 (d, J = 7.6 Hz, 2H), 7.33 (t, 2H), 7.82 ppm (d, J = 8.6 Hz, 2H); ^{13}C NMR (100 MHz, $CDCl_3$): δ = 23.1, 29.3, 29.5, 62.0, 68.1, 70.4, 70.6, 71.5, 72.7, 105.5, 114.3, 125.2, 126.9, 154.8 ppm.

21: TsCl (2.8 g, 14.7 mmol) dissolved in $CHCl_3$ (30 mL) was added dropwise over 20–30 min to a solution of **20** (7.0 g, 13.8 mmol), DMAP (90 mg, 0.74 mmol), and Et_3N (2.5 mL) in CH_2Cl_2 (50 mL). The mixture was stirred for 4 h at room temperature. The reaction mixture was washed with aqueous HCl (0.1 N, 2×100 mL), dried ($MgSO_4$), filtered, and concentrated to dryness. The residue was purified by column chromatography (SiO_2), eluting first with a mixed solvent ($CHCl_3$/Me_2CO = 4:1) to remove the ditosylate and then with another mixed solvent ($CHCl_3$/Me_2CO = 3:2) to recover the product. Concentration in vacuo gave **21** (3.9 g, 43%) as a light-yellow oil. ^{1}H NMR (400 MHz, $CDCl_3$): δ = 1.55–1.75 (m, 8H), 1.93 (m, 4H), 3.42–3.62 (m, 12H), 3.62–3.72 (m, 6H), 4.13 (m, 6H), 6.81 (d, J = 7.6 Hz, 2H), 7.28–7.35 (m, 4H), 7.78 (d, J = 8.3 Hz, 2H), 7.82 ppm (d, J = 8.6 Hz, 2H); ^{13}C NMR (100 MHz, $CDCl_3$): δ = 21.8, 23.1, 29.3, 29.6, 62.1, 68.1, 68.9, 69.5, 70.3, 70.5, 70.7, 71.0, 71.5, 71.6, 72.7, 105.5, 114.3, 125.3, 127.0, 128.2, 130.0, 133.2, 145.0, 154.8 ppm.

22: BZ (4.0 g, 21.7 mmol), **9** (9.0 g, 25.8 mmol), and Et_3N (10 mL) were mixed in PhMe (100 mL). The reaction mixture was heated under reflux for 16 h. After the removal of the solvent by evaporation, the residue was dissolved in CH_2Cl_2 (200 mL), washed with saturated aqueous $NaHCO_3$ (200 mL), dried ($MgSO_4$), filtered, and concentrated to dryness. The residue was purified by column chromatography (SiO_2, CH_2Cl_2/Me_2CO = 1:1). Concentration in vacuo afforded **22** (3.5 g, 45%) as an orange oil. ^{1}H NMR (400 MHz, $CDCl_3$): δ = 3.33 (m, 2H), 3.58–3.78 (m, 14H), 6.68 (m, 4H), 7.35 ppm (m, 4H); ^{13}C NMR (100 MHz, $CDCl_3$): δ = 43.9, 61.9, 69.8, 70.4, 70.5, 70.7, 70.9, 72.9, 113.7, 115.7, 127.4, 129.3, 130.8, 132.2, 145.0, 147.2 ppm.

23: Compound **22** (4.0 g, 11.0 mmol) dissolved in hot PhMe (5 mL) was added to a solution of **21** and Et_3N (2 mL) in hot PhMe (5 mL). The reaction mixture was heated under reflux for 16 h. The solvent was removed by evaporation. The residue was dissolved in CH_2Cl_2 (200 mL), washed with saturated aqueous $NaHCO_3$ (200 mL), dried ($MgSO_4$), filtered, and concentrated to dryness. The residue was purified by column

chromatography (SiO_2), eluting first with EtOAc to remove unreacted **22** and then with a mixed solvent (CH_2Cl_2/Me_2CO = 2:1) to recover the product. Concentration in vacuo afforded **23** (3.3 g, 43%) as an orange oil. ^{1}H NMR (400 MHz, $CDCl_3$): δ = 1.63 (m, 4H), 1.72 (m, 4H), 1.93 (m, 4H), 2.52 (br, 2H), 3.32 (m, 4H), 3.53 (m, 4H), 3.55–3.72 (m, 28H), 4.12 (t, 4H), 6.66 (m, 4H), 6.80 (d, J = 7.6 Hz, 2H), 7.28–7.39 (m, 6H), 7.82 ppm (d, J = 8.6 Hz, 2H); ^{13}C NMR (100 MHz, $CDCl_3$): δ = 23.1, 29.4, 29.6, 43.9, 62.0, 68.1, 69.9, 70.4, 70.5, 70.7, 70.9, 71.6, 72.7, 72.9, 105.5, 113.6, 113.7, 114.3, 125.3, 127.0, 127.3, 129.3, 130.9, 146.9, 154.8 ppm.

24: Compound **23** (3.0 g, 3.5 mmol) and di-*tert*-butyl dicarbonate (3.0 g, 13.7 mmol) were dissolved in Me_2CO (10 mL). The reaction mixture was stirred at room temperature for 3 days. After dilution with EtOAc (100 mL), the reaction mixture was washed with saturated aqueous $NaHCO_3$ (2 × 100 mL), dried ($MgSO_4$), filtered, and concentrated to dryness. The residue was subjected to column chromatography (SiO_2, CH_2Cl_2/Me_2CO = 2:1). Concentration in vacuo gave **24** (2.6 g, 70%) as an orange oil. ^{1}H NMR (400 MHz, $CDCl_3$): δ = 1.45 (s, 18H), 1.63 (m, 4H), 1.72 (m, 4H), 1.93 (m, 4H), 2.55 (br, 2H), 3.53–3.72 (m, 32H), 3.82 (t, 4H), 4.12 (t, 4H), 6.80 (d, J = 7.6 Hz, 2H), 7.27–7.34 (m, 6H), 7.51 (d, J = 8.3 Hz, 4H), 7.82 ppm (d, J = 8.2 Hz, 2H); ^{13}C NMR (100 MHz, $CDCl_3$): δ = 22.9, 28.4, 29.1, 29.4, 31.0, 49.5, 61.7, 61.9, 67.9, 70.3, 70.5, 70.6, 70.7, 71.4, 72.5, 72.9, 80.4, 105.3, 114.3, 125.1, 126.8, 127.2, 127.3, 129.1, 138.0, 141.9, 154.3, 154.7, 206.4 ppm.

25: TsCl (1.0 g, 5.2 mmol) dissolved in CH_2Cl_2 (15 mL) was added dropwise to a solution of **24** (2.4 g, 2.3 mmol), DMAP (40 mg, 0.33 mmol), and triethylamine (1.0 mL) in CH_2Cl_2 (15 mL). The solution was stirred at room temperature for 16 h then subjected directly to column chromatography (SiO_2, EtOAc/CH_2Cl_2 = 1:4). Concentration in vacuo gave **25** (2.5 g, 80%) as a light-yellow oil. ^{1}H NMR (400 MHz, $CDCl_3$): δ = 1.45 (s, 18H), 1.63 (m, 4H), 1.72 (m, 4H), 1.93 (m, 4H), 2.42 (s, 6H), 3.43–3.72 (m, 28H), 3.82 (m, 4H), 4.10–4.18 (m, 8H), 6.80 (d, J = 7.6 Hz, 2H), 7.27–7.34 (m, 10H), 7.51 (d, J = 8.3 Hz, 4H), 7.78 (d, J = 8.4 Hz, 4H), 7.82 ppm (d, J = 8.2 Hz, 2H); ^{13}C NMR (100 MHz, $CDCl_3$): δ = 21.8, 23.1, 28.6, 29.1, 29.4, 31.0, 49.5, 61.7, 61.9, 67.9, 70.3, 70.5, 70.6, 70.7, 71.4, 72.5, 72.9, 80.4, 105.5, 114.5, 125.3, 127.0, 127.4, 127.5, 128.1, 129.3, 130.0, 133.1, 138.2, 142.1, 145.0, 154.5, 154.9, 206.4 ppm.

6: TTF-OH (0.15 g, 0.57 mmol) and **25** (0.80 g, 0.59 mmol) dissolved in dry THF (70 mL) were added to a solution of NaH (0.1 g) and Cs_2CO_3 (0.5 g) in dry THF (50 mL) under an atmosphere of dry argon. The reaction mixture was heated under reflux for 2 days. After cooling to room temperature, NaH was quenched by addition of an aqueous mixed solvent (Me_2CO/H_2O = 9:1, 1 mL). The solution was dried ($MgSO_4$), filtered, and concentrated to dryness. The residue was purified by column chromatography (SiO_2), eluting first with a mixed solvent (CH_2Cl_2/EtOAc = 1:1) to remove unreacted starting material and then with EtOAc to recover the product. Concentration in vacuo gave **6** (0.23 g, 30%) as a yellow oil. ^{1}H NMR (400 MHz, CD_3CN): δ = 1.38 (s, 18H), 1.48–1.63 (m, 8H), 1.82 (m, 4H), 3.32–3.58 (m, 32H), 3.70 (m, 4H), 4.00–4.15 (m, 8H), 6.18–6.25 (m, 2H), 6.81 (m, 2H), 7.22–7.34 (m, 6H), 7.52 (m, 4H), 7.73 ppm (m, 2H); ^{13}C NMR (100 MHz, CD_3CN): δ = 22.8, 27.6, 28.8, 29.3, 49.6, 60.1, 63.5, 67.5, 68.0, 68.2, 68.4, 69.1, 69.2, 69.7, 69.9, 70.0, 70.1, 70.2, 70.3, 70.6, 70.7, 79.8, 72.5, 72.9, 80.4, 105.5, 109.9, 113.7, 116.6, 116.7, 125.5, 126.6, 126.7, 127.6, 127.8, 130.0, 132.9, 134.6, 137.4, 142.4, 154.2, 154.5, 206.4 ppm; MS (ESI): m/z = 1301.2 $[M+Na]^+$.

3·4PF_6: Boc-protected crown ether **5** (0.35 g, 0.27 mmol), **7**·2PF_6 (0.19 g, 0.27 mmol), and **8** (0.07 g, 0.27 mmol) were dissolved in DMF (10 mL). The reaction mixture was transferred to a high-pressure teflon reaction tube, which was then compressed (12 kbar) at room temperature for 3 days. After decompression of the reaction vessel, the reaction mixture was subjected directly to column chromatography (SiO_2), eluting first with EtOAc and Me_2CO to remove the impurities and then with a mixed solvent (MeOH/NH_4Cl (2 M)/$MeNO_2$ = 5:4:1) to recover the product. After the organic solvent was removed by evaporation, **3**·4PF_6 was precipitated by the addition of NH_4PF_6 to the aqueous solution. Filtration and drying under vacuum gave **3**·4PF_6 (0.36 g, 55%) as a green solid. ^{1}H NMR (400 MHz, CD_3CN): δ = 1.30–1.60 (d, 18H), 3.32–4.30 (m, 48H), 5.45–5.70 (m, 8H), 5.82–6.09 (s, 2H), 6.65–6.82 (m, 2H), 7.15–7.70 (m, 18H), 7.80–8.00 (br, 2H), 8.40–9.00 ppm (m, 8H).

1·4PF_6: Boc-protected [2]catenane **3**·4PF_6 (0.10 g, 4.2×10^{-5} mol) and *p*-toluenesulfonic acid monohydrate (80 mg, 4.2×10^{-4} mol) were dissolved in Me_2CO (10 mL). The reaction mixture was heated under reflux for 2.5 h in the dark. After cooling to room temperature, the solvent was removed by evaporation. The residue was dissolved in $MeNO_2$ (50 mL) and washed with an aqueous solution (100 mL) of $NaHCO_3$ (saturated) and NH_4PF_6 (1.0 g). The organic layer was recovered and dried ($MgSO_4$), filtered, and concentrated to dryness. The residue was purified by column chromatography (SiO_2), eluting first with Me_2CO and then with a mixed solvent (MeOH/NH_4Cl (1 M)/$MeNO_2$ = 5:4:1). The green band was collected, and the organic solvent was removed by evaporation. NH_4PF_6 was added to the aqueous solution to effect counterion exchange. The green compound precipitated was recovered by filtration. The green solid was dissolved in Me_2CO, dried ($MgSO_4$), filtered, and concentrated to give **1**·4PF_6 (42 mg, 46%) as a green solid. ^{1}H NMR (400 MHz, CD_3CN): δ = 2.97–3.20 (br, 2H), 3.30–4.00 (m, 42H), 4.00–4.10 (m, 4H), 4.15–4.25 (br, 4H), 5.40–5.75 (m, 8H), 5.98–6.15 (m, 2H), 6.45–6.65 (br, 2H), 6.72 (m, 1H), 6.77–6.88 (br, 3H), 7.20–7.65 (m, 24H), 7.80–9.05 ppm (m, 8H); ^{13}C NMR (100 MHz, CD_3CN): δ = 65.8, 65.9, 68.8–69.4, 70.4–70.7, 70.8–72.3, 107.4, 107.5, 109.0, 114.8–114.8, 126.0–126.4, 126.5, 127.0, 127.3, 127.5–127.8, 131.6–132.4, 136.7–137.5, 144.8–145.2, 145.3–145.9, 146.2–146.7, 155.3–155.6 ppm; MS (ESI): m/z = 946.3 $[M-2PF_6]^{2+}$.

4·4PF_6: Boc-protected crown ether **6** (0.20 g, 0.16 mmol), **7**·2PF_6 (0.13 g, 0.18 mmol), and **8** (49 mg, 0.19 mmol) were dissolved in dry DMF (10 mL). The reaction mixture was transferred to a high-pressure teflon reaction tube, which was then compressed (12 kbar) at room temperature for 3 days. After decompression of the reaction vessel, the reaction mixture was subjected directly to column chromatography (SiO_2), eluting first with EtOAc and Me_2CO to remove the impurities and then with a mixed solvent (MeOH/NH_4Cl (2 M)/$MeNO_2$ = 5:4:1) to recover the product. The green band was collected, and the organic solvent was removed by evaporation. NH_4PF_6 was added to the aqueous solution to effect counterion exchange. The green compound precipitated was recovered by filtration. The compound was dissolved in Me_2CO, dried ($MgSO_4$), and filtered. Concentration in vacuo gave **4**·4PF_6 (0.13 g, 35%) as a green solid. ^{1}H NMR (500 MHz, CD_3CN): δ = 1.20–1.70 (m, 30H), 3.30–3.95 (m, 48H), 4.03–4.15 (m, 8H), 5.48–5.67 (m, 8H), 5.95–6.18 (m, 2H), 6.67–6.86 (m, 6H), 7.10–7.90 (m, 24H), 8.50–9.05 ppm (m, 8H); ^{13}C NMR (125 MHz, CD_3CN): δ = 22.6, 22.7, 27.4, 27.5, 28.5–28.7, 28.9, 29.2, 29.7, 64.0–64.2, 64.3, 67.3–67.4, 67.6–68.5, 69.0, 69.6–70.1, 70.2–70.6, 70.8, 80.0, 105.4, 105.6, 105.8, 107.5, 107.6, 113.5, 113.6, 115.0, 116.5–116.8, 119.4, 119.5, 124.4–125.6, 126.0–126.8, 127.4, 127.7, 127.8, 129.4, 130.4–130.7, 131.1, 132.2, 132.4, 135.6, 137.0, 142.6, 143.3, 143.6–145.0, 145.5, 154.2–154.5, 206.4 ppm.

2·4PF_6: Boc-protected [2]catenane **4**·4PF_6 (0.10 g, 4.2×10^{-5} mol) and *p*-toluenesulfonic acid monohydrate (80 mg, 4.2×10^{-4} mol) were dissolved in Me_2CO (5 mL). The reaction mixture was heated under reflux for 2.5 h. After cooling to room temperature, the solvent was removed by evaporation. The residue was dissolved in $MeNO_2$ (50 mL) and washed with an aqueous solution (100 mL) of $NaHCO_3$ (saturated) and NH_4PF_6 (1.0 g). The organic layer was recovered and dried ($MgSO_4$), filtered, and concentrated to dryness. The residue was purified by column chromatography (SiO_2), eluting first with Me_2CO and then with a mixed solvent (MeOH/NH_4Cl (1 M)/$MeNO_2$ = 5:4:1). The green band was collected. After the organic solvent was removed by evaporation, the insoluble green compound was recovered by filtration. The green solid was dissolved in MeOH, added to water (100 mL), and then NH_4PF_6 was added to effect counterion exchange. The green precipitate was recovered by filtration. The product was dissolved in Me_2CO, dried ($MgSO_4$), and filtered. Concentration in vacuo gave **2**·4PF_6 (48 mg, 50%) as a green solid. ^{1}H NMR (500 MHz, CD_3CN): δ = 1.35 (s, 4H), 1.62–1.72 (m, 6H), 1.92 (overlapping with solvent), 2.98 (s, 2H), 3.23 (s, 2H), 3.38–3.92 (m, 32H), 4.02 (s, 2H), 4.07 (s, 2H), 4.16 (t, 4H), 5.41 (br, 4H), 5.56 (br, 4H), 6.09 (s, 1H), 6.12 (s, 1H), 6.38 (d, J = 7.8 Hz, 2H), 6.60 (d, J = 7.8 Hz, 2H), 6.74 (d, J = 8.2 Hz, 1H), 6.89 (d, J = 8.2 Hz, 1H), 7.12 (d, J = 7.8 Hz, 2H), 7.17 (d, J = 7.8 Hz, 2H), 7.33 (m, 2H), 7.38–7.63 (m, 17H), 7.72 (d, J = 7.4 Hz, 1H), 7.70 (br, 4H), 8.86 ppm (br, 4H); ^{13}C NMR (125 MHz, CD_3CN): δ = 22.6, 22.8, 28.4, 28.5, 28.7, 29.0, 43.0, 43.2, 64.1, 64.3, 67.3, 67.4, 67.6, 67.9, 68.9, 69.0, 69.4, 69.6, 69.7, 69.9, 70.2, 70.3, 70.4, 70.7,

105.6, 105.8, 107.5, 107.7, 112.8, 113.0, 113.5, 113.6, 116.6, 119.2, 119.4, 124.6, 124.8, 125.0, 125.5, 125.9, 126.0, 126.2, 128.5, 128.7, 130.5, 132.2, 132.4, 135.5, 135.6, 143.3, 143.4, 143.9, 144.1, 144.8, 145.0, 147.0, 147.3, 154.2, 154.3 ppm; MS (ESI): $m/z = 944.0$ $[M-2PF_6]^{2+}$.

Acknowledgements

This work was supported by the Microelectronics Advanced Research Corporation (MARCO) and its Focus Center on Functional Engineered NanoArchitectonics (FENA), as well as the Defense Advanced Research Projects Agency (DARPA) and the Center for Nanoscale Innovative Defense (CNID).

[1] a) J.-M. Lehn, *Supramolecular Chemistry*, VCH, Weinheim, **1995**; b) *Comprehensive Supramolecular Chemistry* (Eds.: J.-M. Lehn, J. L. Atwood, J. E. D. Davies, D. D. MacNicol, F. Vögtle), Pergamon, Oxford, **1996**; c) H.-J. Schneider, A. Yatsimirsky, *Principles and Methods in Supramolecular Chemistry*, Wiley-VCH, Weinheim, **2000**; d) J. W. Steed, J. L. Atwood, *Supramolecular Chemistry*, Wiley-VCH, Weinheim, **2000**; for a selection of articles on supramolecular chemistry and self-assembly, see: e) *Science* **2002**, *295*, 2400–2421; f) Y. K. Agrawal, C. R. Sharma, *Rev. Anal. Chem.* **2005**, *24*, 35–74.

[2] a) *Templated Organic Synthesis* (Eds.: F. Diederich, P. J. Stang), Wiley-VCH, Weinheim, **2000**; b) D. H. Busch, N. A. Stephenson, *Coord. Chem. Rev.* **1990**, *100*, 119–154; c) S. Andoson, H. L. Anderson, J. K. M. Sanders, *Acc. Chem. Res.* **1993**, *26*, 469–475; d) G. A. Breault, C. A. Hunter, D. C. Mayers, *Tetrahedron* **1999**, *55*, 5265–5293; e) T. J. Hubin, D. H. Busch, *Coord. Chem. Rev.* **2000**, *200*, 5–52; f) S. J. Rowan, S. J. Cantrill, G. R. L. Cousins, J. K. M. Sanders, J. F. Stoddart, *Angew. Chem.* **2002**, *114*, 938–993; *Angew. Chem. Int. Ed.* **2002**, *41*, 898–952; g) J. F. Stoddart, H.-R. Tseng, *Proc. Natl. Acad. Sci. USA* **2002**, *99*, 4797–4800; h) M.-J. Blanco, J.-C. Chambron, M. C. Jiménez, J.-P. Sauvage, *Top. Stereochem.* **2003**, *23*, 125–173; i) D. H. Busch, *Top. Curr. Chem.* **2005**, *249*, 1–65.

[3] a) G. Schill, *Catenanes, Rotaxanes and Knots*, Academic Press, New York, **1971**; b) D. M. Walba, *Tetrahedron* **1985**, *41*, 3161–3212; c) C. O. Dietrich-Buchecker, J.-P. Sauvage, *Chem. Rev.* **1987**, *87*, 795–810; d) H. W. Gibson, H. Marand, *Adv. Mater.* **1993**, *5*, 11–21; e) D. B. Amabilino, J. F. Stoddart, *Chem. Rev.* **1995**, *95*, 2725–2828; f) R. Jäger, F. Vögtle, *Angew. Chem.* **1997**, *109*, 966–980; *Angew. Chem. Int. Ed. Engl.* **1997**, *36*, 930–944; g) *Molecular Catenanes, Rotaxanes and Knots* (Eds.: J.-P. Sauvage, C. O. Dietrich-Buchecker), Wiley-VCH, Weinheim, **1999**.

[4] a) P. R. Ashton, T. T. Goodnow, A. E. Kaifer, M. V. Reddington, A. M. Z. Slawin, N. Spencer, J. F. Stoddart, C. Vicent, D. J. Williams, *Angew. Chem.* **1989**, *101*, 1404–1408; *Angew. Chem. Int. Ed. Engl.* **1989**, *28*, 1396–1399; b) P.-L. Anelli, N. Spencer, J. F. Stoddart, *J. Am. Chem. Soc.* **1991**, *113*, 5131–5133; c) P.-L. Anelli, P. R. Ashton, R. Ballardini, V. Balzani, M. Delgado, M. T. Gandolfi, T. T. Goodnow, A. E. Kaifer, D. Philp, M. Pietraszkiewicz, L. Prodi, M. V. Reddington, A. M. Z. Slawin, N. Spencer, J. F. Stoddart, C. Vicent, D. J. Williams, *J. Am. Chem. Soc.* **1992**, *114*, 193–218.

[5] a) P. R. Ashton, R. A. Bissell, N. Spencer, J. F. Stoddart, M. S. Tolley, *Synlett* **1992**, 914–918; b) P. R. Ashton, R. A. Bissell, R. Górski, D. Philp, N. Spencer, J. F. Stoddart, M. S. Tolley, *Synlett* **1992**, 919–922; c) P. R. Ashton, R. A. Bissell, N. Spencer, J. F. Stoddart, *Synlett* **1992**, 923–926; d) R. A. Bissell, E. Córdova, A. E. Kaifer, J. F. Stoddart, *Nature* **1994**, *369*, 133–137; e) M. Asakawa, P. R. Ashton, V. Balzani, A. Credi, C. Hamers, G. Mattersteig, M. Montalti, A. N. Shipway, N. Spencer, J. F. Stoddart, M. S. Tolley, M. Venturi, A. J. P. White, D. J. Williams, *Angew. Chem.* **1998**, *110*, 357–361; *Angew. Chem. Int. Ed.* **1998**, *37*, 333–337; f) V. Balzani, A. Credi, G. Mattersteig, O. A. Matthews, F. M. Raymo, J. F. Stoddart, M. Venturi, A. J. P. White, D. J. Williams, *J. Org. Chem.* **2000**, *65*, 1924–1936.

[6] a) A. M. Elizarov, S.-H. Chiu, J. F. Stoddart, *J. Org. Chem.* **2002**, *67*, 9175–9181; b) S. A. Vignon, T. Jarrosson, T. Iijima, H.-R. Tseng, J. K. M. Sanders, J. F. Stoddart, *J. Am. Chem. Soc.* **2004**, *126*, 9884–9885; c) D. S. Marlin, D. G. Cabrera, D. A. Leigh, A. M. Z. Slawin, *Angew. Chem.* **2006**, *118*, 1413–1418; *Angew. Chem. Int. Ed.* **2006**, *45*, 1385–1390.

[7] a) L. Raehm, J.-M. Kern, J.-P. Sauvage, *Chem. Eur. J.* **1999**, *5*, 3310–3317; b) R. Ballardini, V. Balzani, W. Dehaen, A. E. Dell'Erba, F. M. Raymo, J. F. Stoddart, M. Venturi, *Eur. J. Org. Chem.* **2000**, 591–602; c) A. Altieri, F. G. Gatti, E. R. Kay, D. A. Leigh, D. Martel, F. Paolucci, A. M. Z. Slawin, J. K. Y. Wong, *J. Am. Chem. Soc.* **2003**, *125*, 8644–8654; d) I. Poleschak, J.-M. Kern, J.-P. Sauvage, *Chem. Commun.* **2004**, 474–476; e) Y. Liu, A. H. Flood, R. M. Moskowitz, J. F. Stoddart, *Chem. Eur. J.* **2005**, *11*, 369–385.

[8] a) H. Murakami, A. Kawabuchi, K. Kotoo, M. Kunitake, N. Nakashima, *J. Am. Chem. Soc.* **1997**, *119*, 7605–7606; b) A. M. Brouwer, C. Frochot, F. G. Gatti, D. A. Leigh, L. Mottier, F. Paolucci, S. Roffia, G. W. H. Wurpel, *Science* **2001**, *291*, 2124–2128; c) G. Bottari, D. A. Leigh, E. M. Pérez, *J. Am. Chem. Soc.* **2003**, *125*, 13360–13361; d) A. Altieri, G. Bottari, F. Dehez, D. A. Leigh, J. K. Y. Wong, F. Zerbetto, *Angew. Chem.* **2003**, *115*, 2398–2402; *Angew. Chem. Int. Ed.* **2003**, *42*, 2296–2330; e) D.-H. Qu, Q.-C. Wang, J. Ren, H. Tian, *Org. Lett.* **2004**, *6*, 2085–2088; f) D.-H. Qu, Q.-C. Wang, H. Tian, *Angew. Chem.* **2005**, *117*, 5430–5433; *Angew. Chem. Int. Ed.* **2005**, *44*, 5296–5299; g) M. N. Chatterjee, E. R. Kay, D. A. Leigh, *J. Am. Chem. Soc.* **2006**, *128*, 4058–4073.

[9] a) P. R. Ashton, R. Ballardini, V. Balzani, I. Baxter, A. Credi, M. C. T. Fyfe, M. T. Candolfi, M. Gómez-López, M.-V. Martinez-Díaz, A. Piersanti, N. Spencer, J. F. Stoddart, M. Venturi, A. J. P. White, D. J. Williams, *J. Am. Chem. Soc.* **1998**, *120*, 11932–11942; b) P. R. Ashton, R. Ballardini, V. Balzani, A. Credi, K. R. Dress, E. Ishow, C. J. Kleverlaum, O. Kocian, J. A. Preece, N. Spencer, J. F. Stoddart, M. Venturi, S. Wenger, *Chem. Eur. J.* **2000**, *6*, 3558–3574; c) J. D. Badjic, V. Balzani, A. Credi, S. Silvi, J. F. Stoddart, *Science* **2004**, *303*, 1845–1849; d) T. Iijima, S. A. Vignon, H.-R. Tseng, T. Jarrosson, J. K. M. Sanders, F. Marchioni, M. Venturi, E. Apostoli, V. Balzani, J. F. Stoddart, *Chem. Eur. J.* **2004**, *10*, 6375–6392; e) H. Murakami, Nakashima, *J. Am. Chem. Soc.* **2005**, *127*, 15891–15899; f) J. D. Badjic, C. M. Ronconi, J. F. Stoddart, V. Balzani S. Silvi, A. Credi, *J. Am. Chem. Soc.* **2006**, *128*, 1489–1499.

[10] a) V. Balzani, A. Credi, F. M. Raymo, J. F. Stoddart, *Angew. Chem.* **2000**, *112*, 3484–3530; *Angew. Chem. Int. Ed.* **2000**, *39*, 3348–3391; b) A. R. Pease, J. O. Jeppesen, J. F. Stoddart Y. Luo, C. P. Collier, J. R. Heath, *Acc. Chem. Res.* **2001**, *34*, 433–444; c) C. A. Schalley, K. Beizai, F. Vögtle, *Acc. Chem. Res.* **2001**, *34*, 465–476; d) A. H. Flood, R. J. A. Ramirez, W.-Q. Deng, R. P. Muller, W. A. Goddard, J. F. Stoddart, *Aust. J. Chem.* **2004**, *57*, 301–322; e) T. J. Huang, B. Brough, C.-M. Ho, Y. Liu, A. H. Flood, P. A. Bonvallet, H.-R. Tseng, M. Baller, S. Magonov, J. F. Stoddart, *Appl. Phys. Lett.* **2004**, *85*, 5391–5393; f) Y. Liu, A. H. Flood, P. A. Bonvallet, S. A. Vignon, B. H. Northrop, H.-R. Tseng, J. O. Jeppesen, T. J. Huang, B. Brough, M. Baller, S. Magonov, S. D. Solares, W. A. Goddard, C.-M. Ho, J. F. Stoddart, *J. Am. Chem. Soc.* **2005**, *127*, 9745–9759; g) T. D. Nguyen, H.-R. Tseng, P. C. Celestre, A. H. Flood, Y. Liu, J. F. Stoddart, J. I. Zink, *Proc. Natl. Acad. Sci. USA* **2005**, *102*, 10029–10034; h) J. Berná, D. A. Leigh, M. Lumbomska, S. M. Mendoza, E. M. Pérez, P. Rudolf, G. Teobaldi, F. Zerbetto, *Nat. Mater.* **2005**, *4*, 704–710; i) P. M. Mendes, A. H. Flood, J. F. Stoddart, *Appl. Phys. A* **2005**, *80*, 1197–1207; j) A. H. Flood, E. W. Wong, J. F. Stoddart, *Chem. Phys.* **2006**, *324*, 280–290.

[11] a) D. Philp, J. F. Stoddart, *Synlett* **1991**, 445–458; b) D. Philp, J. F. Stoddart, *Angew. Chem.* **1996**, *108*, 1242–1286; *Angew. Chem. Int. Ed. Engl.* **1996**, *35*, 1154–1196; c) J. F. Stoddart, H.-R. Tseng, *Proc. Natl. Acad. Sci. USA* **2002**, *99*, 4797–4800.

[12] a) J. O. Jeppesen, J. Perkins, J. Becher, J. F Stoddart, *Angew. Chem.* **2001**, *113*, 1256–1261; *Angew. Chem. Int. Ed.* **2001**, *40*, 1216–1221; b) J. O. Jeppesen, K. A. Nielsen, J. Perkins, S. A. Vignon, A. D.

Fabio, R. Ballardini, M. T. Gandolfi, M. Venturi, V. Balzani, J. Becher, J. F. Stoddart *Chem. Eur. J.* **2003**, *9*, 2982–3007; c) H.-R. Tseng, S. A. Vignon, J. F. Stoddart, *Angew. Chem.* **2003**, *115*, 1529–1533; *Angew. Chem. Int. Ed.* **2003**, *42*, 1491–1495; d) H.-R. Tseng, S. A. Vignon, P. C. Celestre, J. Perkins, J. O. Jeppesen, A. D. Fabio, R. Ballardini, M. T. Gandolfi, M. Venturi, V. Balzani, J. Becher, J. F. Stoddart, *Chem. Eur. J.* **2004**, *10*, 155–172; e) J. O. Jeppesen, S. Nygaard, S. A. Vignon, J. F. Stoddart, *Eur. J. Org. Chem.* **2005**, 196—220; for model systems, see: f) S. Nygaard, B. W. Laursen, A. H. Flood, C. Hansen, J. O. Jeppesen, J. F. Stoddart, *Chem. Commun.* **2006**, 144–146; g) A. H. Flood, S. Nygaard, B. W. Laursen, J. O. Jeppesen, J. F. Stoddart, *Org. Lett.* **2006**, *8*, 2205–2208.

[13] a) M. Asakawa, P. R. Ashton, V. Balzani, S. E. Boyd, A. Credi, G. Mattersteig, S. Menzer, M. Montalti, F. M. Raymo, C. Ruffilli, J. F. Stoddart, M. Venturi, D. J. Williams, *Eur. J. Org. Chem.* **1999**, 985–994; b) R. Ballardini, V. Balzani, A. D. Fabio, M. T. Gandolfi, J. Becher, J. Lau, M. B. Nielsen, J. F. Stoddart, *New J. Chem.* **2001**, *25*, 293–298; c) S. A. Vignon, J. Wong, H.-R. Tseng, J. F. Stoddart, *Org. Lett.* **2004**, *6*, 1095–1098; d) S. A. Vignon, J. F. Stoddart, *Collect. Czech. Chem. Commun.* **2005**, *10*, 1493–1576.

[14] a) B. Odell, M. V. Reddington, A. M. Z. Slawin, N. Spencer, J. F. Stoddart, D. J. Williams, *Angew. Chem.* **1988**, *100*, 1605–1608; *Angew. Chem. Int. Ed. Engl.* **1988**, *27*, 1547–1550; b) C. L. Brown, D. Philp, J. F. Stoddart, *Synlett* **1991**, 462–464; c) M. Asakawa, W. Dehaen, G. L'abbé, S. Menzer, J. Nouwen, F. M. Raymo, J. F. Stoddart, D. J. Williams, *J. Org. Chem.* **1996**, *61*, 9591–9595; d) G. Doddi, G. Ercolani, P. Mencarelli, A. Piermattei, *J. Org. Chem.* **2005**, *70*, 3761–3764.

[15] a) D. Philp, A. M. Z. Slawin, N. Spencer, J. F. Stoddart, D. J. Williams, *J. Chem. Soc. Chem. Commun.* **1991**, 1584–1586; b) M. Asakawa, P. R. Ashton, V. Balzani, A. Credi, G. Mattersteig, O. A. Matthews, M. Montalti, N. Spencer, J. F. Stoddart, M. Venturi, *Chem. Eur. J.* **1997**, *3*, 1992–1996; c) M. B. Nielsen, J. O. Jeppesen, J. Lau, C. Lomholt, D. Damgaard, J. P. Jacobsen, J. Becher, J. F. Stoddart, *J. Org. Chem.* **2001**, *66*, 3559–3563.

[16] a) M. V. Reddington, A. M. Z. Slawin, N. Spencer, J. F. Stoddart, C. Vicent, D. J. Williams, *J. Chem. Soc. Chem. Commun.* **1991**, 630–634; b) P. R. Ashton, D. Philp, N. Spencer, J. F. Stoddart, D. J. Williams, *J. Chem. Soc. Chem. Commun.* **1994**, 181–184; c) P. R. Ashton, R. Ballardini, V. Balzani, S. E. Boyd, A. Credi, M. T. Gandolfi, M. Gómez-López, S. Iqbal, D. Philp, J. A. Preece, L. Prodi, H. G. Ricketts, J. F. Stoddart, M. S. Tolley, M. Venturi, A. J. P. White, D. J. Williams, *Chem. Eur. J.* **1997**, *3*, 152–170.

[17] a) P. R. Ashton, B. Odell, M. V. Reddington, A. M. Z. Slawin, J. F. Stoddart, D. J. Williams, *Angew. Chem.* **1988**, *100*, 1608–1611; *Angew. Chem. Int. Ed. Engl.* **1988**, *27*, 1550–1553; b) P.-L. Anelli, P. R. Ashton, N. Spencer, A. M. Z. Slawin, J. F. Stoddart, D. J. Williams, *Angew. Chem.* **1991**, *103*, 1052–1054; *Angew. Chem. Int. Ed. Engl.* **1991**, *30*, 1036–1039; c) K. N. Houk, S. Menzer, S. P. Newton, F. M. Raymo, J. F. Stoddart, *J. Am. Chem. Soc.* **2001**, *123*, 9264–9267.

[18] a) C. P. Collier, G. Mattersteig, E. W. Wong, Y. Luo, K. Beverly, J. Sampaio, F. M. Raymo, J. F. Stoddart, J. R. Heath, *Science* **2000**, *289*, 1172–1175; b) C. P. Collier, J. O. Jeppesen, Y. Luo, J. Perkins, E. W. Wong, J. R. Heath, J. F. Stoddart, *J. Am. Chem. Soc.* **2001**, *123*, 12632–12641; c) Y. Luo, C. P. Collier, J. O. Jeppesen, K. A. Nielsen, E. DeIonno, G. Ho, J. Perkins, H.-R. Tseng, T. Yamamoto, J. F. Stoddart, J. R. Heath, *ChemPhysChem* **2002**, *3*, 519–525; d) H. B. Yu, Y. Luo, K. Beverly, J. F. Stoddart, H.-R. Tseng, J. R. Heath, *Angew. Chem.* **2003**, *115*, 5884–5889; *Angew. Chem. Int. Ed.* **2003**, *42*, 5706–5711; e) M. R. Diehl, D. W. Steuerman, H.-R. Tseng, S. A. Vignon, A. Star, P. C. Celestre, J. F. Stoddart, J. R. Heath, *ChemPhysChem* **2003**, *4*, 1335–1339; f) H.-R. Tseng, D. Wu, N. X. Fang, X. Zhang, J. F. Stoddart, *ChemPhysChem* **2004**, *5*, 111–116; g) A. H. Flood, A. J. Peters, S. A. Vignon, D. W. Steuerman, H.-R. Tseng, S. Kang, J. R. Heath, J. F. Stoddart, *Chem. Eur. J.* **2004**, *10*, 6558–6564; h) A. H. Flood, J. F. Stoddart, D. W. Steuerman, J. R. Heath, *Science* **2004**, *306*, 2055–2056; i) S. S. Jang, Y. H. Jang, Y.-H. Kim, W. A. Goddard, J. W. Choi, J. R. Heath, B. W. Laursen, A. H. Flood, J. F. Stoddart, K. Nørgaard, T. Bjørnholm, *J. Am. Chem. Soc.* **2005**, *127*, 14804–14816; j) R. Beckman, K. Beverly, A. Boukai, Y. Bunimovich, J. W. Choi, E. DeIonno, J. Green, E. Johnston-Halperin, Y. Luo, B. Sheriff, J. F. Stoddart, J. R. Heath, *Faraday Discuss.* **2006**, *131*, 9–22; k) E. DeIonno, H.-R. Tseng, D. D. Harvey, J. F. Stoddart, J. R. Heath, *J. Phys. Chem. B* **2006**, *110*, 7609–7612.

[19] D. A. Leigh, J. K. Y. Wong, F. Dehez, F. Zerbetto, *Nature* **2003**, *424*, 174–179.

[20] W.-Q. Deng, A. H. Flood, J. F. Stoddart, W. A. Goddard, *J. Am. Chem. Soc.* **2005**, *127*, 15994–15995.

[21] D. W. Steuerman, H.-R. Tseng, A. J. Peters, A. H. Flood, J. O. Jeppesen, K. A. Nielsen, J. F. Stoddart, J. R. Heath, *Angew. Chem.* **2004**, *116*, 6648–6653; *Angew. Chem. Int. Ed.* **2004**, *43*, 6486–6491.

[22] Here we are correlating the K_a values for the 1:1 complexes formed between $CBPQT^{4+}$ and the recognition sites in model compounds with the relative populations for the encirclement of these same recognition sites in the tristable [2]catenane.

[23] R. Castro, K. R. Nixon, J. D. Evanseck, A. E. Kaifer, *J. Org. Chem.* **1996**, *61*, 7298–7303.

[24] J. W. Choi, A. H. Flood, D. W. Steuerman, S. Nygaard, A. B. Braunschweig, N. N. P. Moonen, B. W. Laursen, Y. Luo, E. DeIonno, A. J. Peters, J. O. Jeppesen, K. Xu, J. F. Stoddart, J. R. Heath, *Chem. Eur. J.* **2006**, *12*, 261–279.

[25] a) E. Córdova, R. A. Bissell, N. Spencer, P. R. Ashton, J. F. Stoddart, A. E. Kaifer, *J. Org. Chem.* **1993**, *58*, 6440–6552; b) E. Córdova, R. A. Bissell, A. E. Kaifer, *J. Org. Chem.* **1995**, *60*, 1033–1038.

[26] T. Ikeda, E. Hirota, T. Ooya, N. Yui, *Langmuir* **2001**, *17*, 234–238.

[27] P. R. Ashton, J. Huff, S. Menzer, I. W. Parsons, J. A. Preece, J. F. Stoddart, M. S. Tolley, A. J. P. White, D. J. Williams, *Chem. Eur. J.* **1996**, *2*, 123–136.

[28] a) L. R. Melby, H. D. Hartzler, W. A. Sheppard, *J. Org. Chem.* **1974**, *39*, 2456–2458; b) R. Andrew, J. Garin, J. Orduna, M. Savirón, J. Cousseau, A. Gorgues, V. Morisson, T. Nozdryn, J. Becher, R. P. Clausen, M. R. Bryce, P. J. Skabara, W. Dehaen, *Tetrahedron Lett.* **1994**, *35*, 9243–9246.

[29] D. B. Amabilino, P. R. Ashton, A. S. Reder, N. Spencer, J. F. Stoddart, *Angew. Chem.* **1994**, *106*, 1316–1319; *Angew. Chem. Int. Ed. Engl.* **1994**, *33*, 1286–1290.

[30] N. Miyashita, A. Yoshikoshi, P. A. Grieco, *J. Org. Chem.* **1977**, *42*, 3772–3774.

[31] a) S. Hünig, G. Kiesslich, H. Quast, D. Scheutzow, *Justus Liebigs Ann. Chem.* **1973**, 310–323; b) G. Schukat, E. Fanghänel, *J. Prakt. Chem.* **1985**, *327*, 767–774.

[32] a) R. Ballardini, V. Balzani, A. Credi, C. L. Brown, R. E. Gillard, M. Montalti, D. Philp, J. F. Stoddart, M. Venturi, A. J. P. White, B. J. Williams, D. J. Williams, *J. Am. Chem. Soc.* **1997**, *119*, 12503–12513; b) P. R. Ashton, V. Balzani, J. Becher, A. Credi, M. C. T. Fyfe, G. Mattersteig, S. Menzer, M. B. Nielsen, F. M. Raymo, J. F. Stoddart, M. Venturi, D. J. Williams, *J. Am. Chem. Soc.* **1999**, *121*, 3951–3957.

[33] P.-L. Anelli, P. R. Ashton, R. Ballardini, V. Balzani, M. Delgado, M. T. Gandolfi, T. T. Goodnow, A. E. Kaifer, D. Philp, M. Pietraszkiewicz, L. Prodi, M. V. Reddington, A. M. Z. Slawin, N. Spencer, J. F. Stoddart, C. Vicent, D. J. Williams, *J. Am. Chem. Soc.* **1992**, *114*, 193–218.

[34] P. Chandrasekhar, R. W. Gumbs, *J. Electrochem. Soc.* **1991**, *138*, 1337–1346.

[35] A. J. Bard, L. R. Faulkner, *Electrochemical Methods: Fundamentals and Applications*, 2nd ed., Wiley, New York, **2001**.

Received: October 23, 2006
Published online: December 5, 2006

